Please cite this article as:
V. Laheri, P. Hao, F.A. Gilabert.
"Efficient non-iterative modelling of pressure-dependent plasticity using paraboloidal yield criterion".
International Journal of Mechanical Sciences (2021), DOI: https://doi.org/10.1016/j.ijmecsci.2021.106988
Received: 18 Jul 2021, Revised: 25 Oct 2021, Accepted: 5 Dec 2021.

Efficient non-iterative modelling of pressure-dependent plasticity using paraboloidal yield criterion

V. Laheri[a], P. Hao[a,b], F. A. Gilabert[a,*]

[a]*Ghent University, Department of Materials, Textiles and Chemical Engineering, Tech Lane Ghent Science Park - Campus A, Technologiepark-Zwijnaarde 46, 9052 Zwijnaarde, Belgium.*
[b]*SIM M3 Program, 9052 Zwijnaarde, Belgium.*

Abstract

A full understanding of the non-linear mechanical response of the polymer is essential for fibre-reinforced polymer composite design because an explicit definition of constitutive material models for the constituents (fibres, matrix, and interface) are prerequisite in micromechanical simulations. Unlike ductile metals, the material behaviour of polymer matrix is characterised by plasticity theories influenced by a combination of distortional and spherical energy dissipation. In this respect, an elastoplastic thermodynamic continuum model derivation is proposed using the paraboloidal yield criterion under isothermal conditions. A non-iterative scheme is developed for the numerical computation of the plastic strain increment multiplier. Both associated and non-associated flow rules are investigated following classical plasticity loading-unloading conditions. It thereby, evades conventional computationally demanding iterative process by replacing it with an exact determination of plastic strain increment. This novel approach highly improves the computational efficiency algorithmically. The real-sized numerical models are investigated and the comparison between simulated and experimental results shows the reliability and unprecedented accuracy of the proposed elastoplastic mathematical model.

*Corresponding author:
Email address: Fran.Gilabert@UGent.be (F. A. Gilabert)

Please cite this article as:
V. Laheri, P. Hao, F.A. Gilabert.
"Efficient non-iterative modelling of pressure-dependent plasticity using paraboloidal yield criterion".
International Journal of Mechanical Sciences (2021), DOI: https://doi.org/10.1016/j.ijmecsci.2021.106988
Received: 18 Jul 2021, Revised: 25 Oct 2021, Accepted: 5 Dec 2021.

Nomenclature

Operators

$\Delta\square$	increment operator
$\dot{\square}$	time-rate change operator
$\square^{\top}$	transpose operator
$\square'$	deviatoric operator
$\square^{K}$	hydrostatic operator
$\square^{e}$	elastic part denotation
$\square^{p}$	plastic part denotation
$\square_{t}$	tensile denotation
$\square_{c}$	compressive denotation
$\square^{tr}$	predicted or trail state
$\square_{homog}$	homogenised state
$\square_{inst}$	instantaneous

Symbols and Variables

ν	Poisson's ratio
ν^{p}	plastic Poisson's ratio
Ψ	Helmholtz's energy function
ϕ	yield function
g	potential function
α_{0}	pressure-dependent coefficient
$\boldsymbol{\varepsilon}$	2nd order strain tensor matrix
$\boldsymbol{\sigma}$	2nd order stress tensor matrix
$\mathbb{C}$	4th order tangent modulus tensor
E	Young's elastic modulus
μ	shear modulus
κ	sulk modulus
h	linear hardening modulus
β	stress due to hardening
α	strain-like parameter

Please cite this article as:
V. Laheri, P. Hao, F.A. Gilabert.
"Efficient non-iterative modelling of pressure-dependent plasticity using paraboloidal yield criterion".
International Journal of Mechanical Sciences (2021), DOI: https://doi.org/10.1016/j.ijmecsci.2021.106988
Received: 18 Jul 2021, Revised: 25 Oct 2021, Accepted: 5 Dec 2021.

$\overline{\epsilon}^p$	equivalent plastic strain
I_1	1st invariant of the stress tensor
$\overline{\sigma}$	equivalent stress
σ_t	yield stress in tension
σ_c	yield stress in compression
$\mathbf{N}$	projected gradient of flow tensor
$\hat{n}$	scalar quantity (Frobenius norm) of the projected flow tensor
$\boldsymbol{\eta}$	flow normal
$\Delta\gamma$	plastic strain increment
$\mathcal{D}_{int}$	reduced internal dissipation
$\mathbf{I}$	2nd identity tensor
$\mathbb{I}^{sym}$	4th symmetric identity tensor
$\bar{\mathbb{I}}$	4th hydrostatic operator tensor
$\mathbb{P}$	4th projection tensor
V	volume
ℓ_{elem}	element length
dt	time increment

Keywords: Continuum mechanics, computational methods, finite element, flow-rule, paraboloidal yield criterion, pressure-dependent elastoplasticity, polymer matrix

1. Introduction

Many efforts are being made to improve the mechanical performance of fibre-reinforced polymer composites, and multiscale analysis based on finite element modelling is nowadays a very popular approach [34]. At the lower scales, this approach relies on micromechanical models using representative volume elements (RVE) combined with homogenisation techniques to provide a detailed expression of the mechanical response. Apart from the application-oriented designs by means of the optimized usage of fibres, the mechanical behaviour of polymer matrices is still a key point in the overall composite performance. Due to the difference in the transverse mechanical responses of fibres and matrix to

Please cite this article as:
V. Laheri, P. Hao, F.A. Gilabert.
"Efficient non-iterative modelling of pressure-dependent plasticity using paraboloidal yield criterion".
International Journal of Mechanical Sciences (2021), DOI: https://doi.org/10.1016/j.ijmecsci.2021.106988
Received: 18 Jul 2021, Revised: 25 Oct 2021, Accepted: 5 Dec 2021.

the mechanical loading, the matrix is usually under triaxial stress state inhibiting its plasticity and strength [18]. Unreinforced resin at microstructural level is brittle in tension while exhibits considerable plasticity in compression and pure shear [28]. This demands appropriate plastic models with realistic yield criterion and robust computational procedure to deal with a highly non-linear material response accurately and efficiently. So also, the plastic initiation and further flow are highly sensitive of strain-rate and temperature. This work presents an efficient and accurate algorithmic scheme to compute the rate and temperature independent elastoplastic evolution of the polymer matrix without resorting to computationally expensive iterative processes.

Based on the elastic shear strain energy theory, von Mises plasticity projects a cylindrical surface in the triaxial principal stress coordinates rendering it suitable for ductile materials, like metals. Due to the incompressibility at plastic yielding allowing permanent volumetric deformation as an effect of the equal yield strength under tension and compression, Du Bois *et al.* [5] particularly suggests the preclusion of von Mises plasticity for polymers. In an extensive research on the several types of plasticity models that have been proposed for the polymers, Ghorbel [21] emphasises on the importance of the hydrostatic pressure on polymer plastic yielding. It therefore renders yield models independent of pressure like von Mises and Tresca inadequate.

It is established that the polymer plasticity depends on the spherical and distortional strain energies, wherein Mascarenhas *et al.* [31] recommends to use conic or parabolic design criteria for polymer yielding. Besides Wronski and Pick [59] also suggests the yield criteria of conical, paraboloidal or pyramidal types as the best correlation for tension-compression asymmetry. The spherical component results from the hydrostatic or pressure-dependent part, while the distortional component is caused by the deviatoric or octahedral shear part of the stress state. The phenomonological model to express rate-dependent viscoplasticity developed by Boyce *et al.* [1, 7] has also been extensively adopted in various modifications by numerous researchers, like Canal *et al.* [9], Hara and Shizawa [24], Johnsen *et al.* [27], Kriari and Doghri [30], Poulain *et al.* [39], Van der Giessen and team [38, 44, 48, 60, 61] and many more. The exponential model

Please cite this article as:
V. Laheri, P. Hao, F.A. Gilabert.
"Efficient non-iterative modelling of pressure-dependent plasticity using paraboloidal yield criterion".
International Journal of Mechanical Sciences (2021), DOI: https://doi.org/10.1016/j.ijmecsci.2021.106988
Received: 18 Jul 2021, Revised: 25 Oct 2021, Accepted: 5 Dec 2021.

of shear strength evolution based on the constant molecular chain movement and entanglement during deformation accurately describes the tension and compression behaviour accurately but overestimate the shear strength when compared to experimental findings [21]. It also requires definition of many fitting parameters for the prediction and fails to determine yield points.

Common standard pressure-dependent yield criteria to describe polymer plasticity are the Drucker-Prager theory used by Du Bois *et al.* [5], Duncan *et al.* [17], Seltzer *et al.* [45], Pulungan *et al.* [40] and de Sousa Junior *et al.* [14] which is primarily based on soil mechanics and soil plasticity analysis [16]. The Mohr-Coulomb plasticity yield theory employed by Bowden and Jukes [6], Totry *et al.* [51, 52], and Gonzáleza and LLorca [22] is also extensively based on soil mechanics and has been classically used for modelling the plastic flow of geomaterials and other cohesive frictional materials, like concrete [13]. The modified von Mises yield criterion used by Ongchin and Sternstein [36], Donato and Bianchi[15] and pressure-modified Tresca used by Parks *et al.* [37] incorporating tension-compression asymmetry and pressure stresses are insufficient to express plasticity in polymeric materials due to their linear functionality like Drucker-Prager and Mohr-Coulomb. These yield criteria are supported on the consideration of distinctly larger yield stresses for pure compression than for pure tension and they project conical yield surface in the triaxial principal stress coordinates. The paraboloidal yield criterion propounded by Tschoegl [53] representing a paraboloid in the triaxial principal stress coordinates system can also be adopted to describe pressure-dependent plasticity.

These yield criteria meet the requirement for convexity in pure tensile and an open surface in pure compressive octants since the yielding does not ordinarily occur under hydrostatic compression at reasonably similar pressures as it occurs in tension [53]. Besides, the paraboloidal yield surface also avoids angular apex in the pure tensile octant. The hydrostatic tensile stress in the polymer matrix combined with strain energy density and paraboloidal yield criterion led to the initial failure where von Mises criterion was unsuitable was inferred by Fiedler *et al.* [19]. Besides being mathematically stable, the model aptly describes void nucleation and void cavitation due to hydrostatic stress while deviatoric

Please cite this article as:
V. Laheri, P. Hao, F.A. Gilabert.
"Efficient non-iterative modelling of pressure-dependent plasticity using paraboloidal yield criterion".
International Journal of Mechanical Sciences (2021), DOI: https://doi.org/10.1016/j.ijmecsci.2021.106988
Received: 18 Jul 2021, Revised: 25 Oct 2021, Accepted: 5 Dec 2021.

stress is responsible for plastic deformation [43]. Therefore, the paraboloidal yield criterion as a quadratic non-homogenous polynomial yield stress function with tension-compression asymmetry becomes more suitable for describing the pressure-dependent plasticity of polymers.

The paraboloidal yield criteria was primarily used by Raghava *et al.* in their series of journal publications [8, 41, 42] for describing polymer plasticity based on constitutive model for uni-dimensional extension. Singh *et. al.* [47] employs paraboloidal yield criterion for the reduced order multiscale modelling of FRP composites with the tangent modulus computed by the perturbation scheme. The elastoplastic computational implementation of the paraboloidal yielding model for epoxy matrices developed by Melro *et al.* [32] has been extensively employed to model the matrix plasticity for RVEs of various composite models recurringly in [2, 3, 20, 25, 33–35, 50, 54–56]. The implementation computes plastic strain increment using a computationally demanding approximation technique based on Newton-Raphsons iterative method that does not always succeed under very large deformations. Several authors [10, 46, 49, 57] have proposed modifications and improvements to the Newton-Raphson method, which are capable of improving the convergence behaviour experienced in the finite element iteration.

To the best of the authors' knowledge, the commercial and non-commercial FEM/FEA software are typically devoid of an elastoplastic model for incorporating the paraboloidal yield criterion. Therefore, it becomes imperative to contrive an efficient computational technique for implementing the constitutive elastoplastic model using the continuum approach to feed the software as a user-defined material model.

This research aims at developing an efficient and exact implementation of the rate and temperature-independent elastoplastic constitutive model with the paraboloidal plasticity theory. With this novel implementation, the plastic strain increment multiplier ($\Delta\gamma$) for both associated and non-associated flow rules are unambiguously calculated using a non-iterative scheme with unprecedented accuracy. The paper also aims at reviewing the differences in the simulation results carried out on the commercial FEM software.

For verification, the proposed implementation is numerically investigated in

Please cite this article as:
V. Laheri, P. Hao, F.A. Gilabert.
"Efficient non-iterative modelling of pressure-dependent plasticity using paraboloidal yield criterion".
International Journal of Mechanical Sciences (2021), DOI: https://doi.org/10.1016/j.ijmecsci.2021.106988
Received: 18 Jul 2021, Revised: 25 Oct 2021, Accepted: 5 Dec 2021.

three levels of benchmark examples: (i) a single-element test to observe its functionality in comparison to the experimental results and to verify its applicability in real-size specimens for (ii) compression test of cylinder and (iii) tension test using dog-bone. The proposed procedure to evaluate the plastic increment diminishes the computational time and avoids the risk of aggregating approximation errors that lead to convergence solver issues.

2. Continuum mechanics

The continuum approach to determine the constitutive relationship of elastoplastic behaviour of the polymer material is employed. The Claussius-Dunhems entropy inequality for isothermal process is given by

$$\boldsymbol{\sigma} : \dot{\boldsymbol{\varepsilon}} - \dot{\Psi} \geqslant 0, \tag{1}$$

where $\boldsymbol{\sigma}$ is the 2$^{\text{nd}}$ order stress tensor and $\dot{\boldsymbol{\varepsilon}}$ is the time rate change of 2$^{\text{nd}}$ order strain tensor $\boldsymbol{\varepsilon}$. $\dot{\Psi}$ is the time rate change of Helmholtz energy function Ψ which considers the total energy in elastoplasticity with isotropic hardening h and it can be written as

$$\Psi\left(\boldsymbol{\varepsilon}^e, \alpha\right) = \underbrace{\mu \|\boldsymbol{\varepsilon}'\|^2 + \tfrac{1}{2}\kappa \left(\boldsymbol{\varepsilon} : \mathbf{I}\right)^2}_{\Psi^e(\boldsymbol{\varepsilon}^e)} + \underbrace{\tfrac{1}{2} h \alpha^2}_{\Psi^p(\alpha)}, \tag{2}$$

where superscripts "e" and "p" account for elastic and plastic parts, respectively and $\mathbf{I}$ is termed as identity matrix. The material parameters μ and κ are the shear and the bulk moduli of elasticity, respectively. The coefficient α is the strain-like parameter, the increment of which is related to equivalent plastic strain increment $\Delta\overline{\epsilon}^p$ defined as the scalar transformation of deviatoric plastic strain tensor

$$\Delta\alpha = \Delta\overline{\epsilon}^p = \sqrt{\frac{2}{3}\,\Delta\boldsymbol{\varepsilon}^{p\prime} : \Delta\boldsymbol{\varepsilon}^{p\prime}}, \tag{3}$$

where $\Delta\boldsymbol{\varepsilon}^{p\prime}$ is isochoric (deviatoric) increment of plastic strain.

In view of its importance for mechanics, an arbitrary 2$^{\text{nd}}$ tensor $\mathbf{T}$ can be

Please cite this article as:
V. Laheri, P. Hao, F.A. Gilabert.
"Efficient non-iterative modelling of pressure-dependent plasticity using paraboloidal yield criterion".
International Journal of Mechanical Sciences (2021), DOI: https://doi.org/10.1016/j.ijmecsci.2021.106988
Received: 18 Jul 2021, Revised: 25 Oct 2021, Accepted: 5 Dec 2021.

deccomposed into the spherical or hydrostatic $\mathbf{T}^K$ and deviatoric or volume preserving or shape changing $\mathbf{T}'$ parts as follows

$$\mathbf{T}^K = \frac{1}{3}\,(\mathbf{T}:\mathbf{I})\,\mathbf{I}, \qquad \mathbf{T}' = \mathbf{T} - \mathbf{T}^K. \tag{4}$$

The ":" operator stands for the scalar product of 2nd order tensors, also referred to as the double contraction or double inner product and it is given by

$$\mathbf{A}:\mathbf{B} = A_{ij}\,B_{ij},$$

where $\mathbf{A}$ and $\mathbf{B}$ are two generic 2nd order tensors with indices i and j along the Cartesian coordinate axes.

2.1. Yield Criterion

The paraboloidal yield criterion as a function of stress tensor is mathematically represented by

$$\phi(\boldsymbol{\sigma}) = \overline{\sigma}^2 - (\sigma_t - \sigma_c)\,I_1 - \sigma_t\,\sigma_c, \tag{5}$$

where $\overline{\sigma} = \sqrt{\frac{3}{2}\,\boldsymbol{\sigma}':\boldsymbol{\sigma}'} = \sqrt{3J_2}$ is the equivalent (von Mises) stress derived from the second invariant J_2 of deviatoric stress. The component of pressure-dependent term $I_1 = \boldsymbol{\sigma}:\mathbf{I} = -3p$ is the first invariant of stress tensor, where p is the hydrostatic pressure. The material parameters σ_t and σ_c are the yield stresses in tension and compression, respectively.

2.2. Constitutive modelling

The plastic flow theory describes the additive decomposition of the material deformation (multiplicative decomposition when expressed in terms of deformation gradient) into its elastic and plastic components

$$\boldsymbol{\varepsilon} = \boldsymbol{\varepsilon}^e + \boldsymbol{\varepsilon}^p. \tag{6}$$

Owing to the associative split of strain, the entropy inequality (1) can be

Please cite this article as:
V. Laheri, P. Hao, F.A. Gilabert.
"Efficient non-iterative modelling of pressure-dependent plasticity using paraboloidal yield criterion".
International Journal of Mechanical Sciences (2021), DOI: https://doi.org/10.1016/j.ijmecsci.2021.106988
Received: 18 Jul 2021, Revised: 25 Oct 2021, Accepted: 5 Dec 2021.

expressed in the form of material-time derivative as follows

$$\boldsymbol{\sigma} : (\dot{\boldsymbol{\varepsilon}}^e + \dot{\boldsymbol{\varepsilon}}^p) - \left(\frac{\partial \Psi^e}{\partial \boldsymbol{\varepsilon}^e} : \dot{\boldsymbol{\varepsilon}}^e + \frac{\partial \Psi^p}{\partial \alpha} \dot{\alpha} \right) \geqslant 0. \tag{7}$$

From the statement of Coleman-Noll [12], the relation for the available free process variable $\dot{\boldsymbol{\varepsilon}}^e$ must be fulfilled. Hence, the constitutive modelling is carried out with the consideration of linear elastic initiation given by

$$\boldsymbol{\sigma} = \frac{\partial \Psi^e}{\partial \boldsymbol{\varepsilon}^e} = 2\mu\, \boldsymbol{\varepsilon}^{e\prime} + \kappa(\boldsymbol{\varepsilon}^e : \mathbf{I})\, \mathbf{I}. \tag{8}$$

The stress can be further additively decomposed into its devaitoric $\boldsymbol{\sigma}' = 2\mu\boldsymbol{\varepsilon}^{e\prime}$ and hydrostatic $\boldsymbol{\sigma}^K = 3\kappa\boldsymbol{\varepsilon}^{eK}$ components.

The elastic tangent modulus, $\mathbb{C}^e$ is a 4$^{\text{th}}$ order tensor derivative of elastic stress with respect to elastic strain given by

$$\mathbb{C}^e = \frac{\partial^2 \Psi^e}{\partial \boldsymbol{\varepsilon}^e\, \partial \boldsymbol{\varepsilon}^e} = \frac{\partial \boldsymbol{\sigma}^e}{\partial \boldsymbol{\varepsilon}^e} = 2\mu\, \mathbb{P} + \kappa \bar{\mathbb{I}}, \tag{9}$$

where $\bar{\mathbb{I}}$ is referred to as the hydrostatic operator, and $\mathbb{P}$ is the projection tensor referred to as the deviatoric operator in 4$^{\text{th}}$ order each. The definitions for these 4$^{\text{th}}$ order tensors related to the 2$^{\text{nd}}$ order identity matrix are as follows

$$\mathbb{I}^{sym} = \frac{1}{2} \left[(\mathbf{I} \otimes \mathbf{I})^{\overset{23}{\top}} + \left((\mathbf{I} \otimes \mathbf{I})^{\overset{23}{\top}} \right)^{\overset{24}{\top}} \right], \tag{10}$$

$$\bar{\mathbb{I}} = \mathbf{I} \otimes \mathbf{I}, \tag{11}$$

$$\text{and} \quad \mathbb{P} = \mathbb{I}^{sym} - \frac{1}{3} \bar{\mathbb{I}}, \tag{12}$$

where "$\top$" is the transpose operator and the numbers overhead it represents the indices being transposed. $\mathbb{I}^{sym}$ is a symmetric 4$^{\text{th}}$ order identity tensor.

The reduced internal dissipation, which is still unfulfilled in the inequality (7) can be written as

$$\mathcal{D}_{int} := \boldsymbol{\sigma} : \dot{\boldsymbol{\varepsilon}}^p - \beta\, \dot{\alpha} \geqslant 0, \tag{13}$$

Please cite this article as:
V. Laheri, P. Hao, F.A. Gilabert.
"Efficient non-iterative modelling of pressure-dependent plasticity using paraboloidal yield criterion".
International Journal of Mechanical Sciences (2021), DOI: https://doi.org/10.1016/j.ijmecsci.2021.106988
Received: 18 Jul 2021, Revised: 25 Oct 2021, Accepted: 5 Dec 2021.

where $\beta = \partial\Psi^p/\partial\alpha = h\alpha$ is the conjugate internal variable associated to stress due to hardening.

The paraboloidal yield criterion for isotropic hardening can be rewritten as

$$\phi(\boldsymbol{\sigma}, \beta) = \overline{\sigma}^2 - (\sigma_t - \sigma_c)I_1 - (\sigma_t + \beta)(\sigma_c + \beta). \tag{14}$$

The reduced internal dissipation inequality (13) can be reformulated in an optimisation problem, tending to stationarity as follows

$$\mathcal{L}(\boldsymbol{\sigma}, \beta, \Delta\gamma) = -\mathcal{D}_{int} + \frac{\Delta\gamma}{\Delta t}\phi(\boldsymbol{\sigma}, \beta) \rightarrow stat., \tag{15}$$

with the Lagrange multiplier $\Delta\gamma$ as the increment of plastic strain.

The flow rule for the evolution of the plastic strain can thus, be computed as

$$\frac{\partial\mathcal{L}}{\partial\boldsymbol{\sigma}} = 0 \qquad \Rightarrow \qquad \Delta\boldsymbol{\varepsilon}^p = \Delta\gamma\frac{\partial\phi}{\partial\boldsymbol{\sigma}} = \Delta\gamma\,\boldsymbol{\eta}, \tag{16}$$

where $\boldsymbol{\eta} = \frac{\partial\phi}{\partial\boldsymbol{\sigma}}$ is the yield surface normal.

The evolution of internal strain-like variable can be computed as

$$\frac{\partial\mathcal{L}}{\partial\beta} = 0 \qquad \Rightarrow \qquad \Delta\alpha = \Delta\gamma\frac{\partial\phi}{\partial\beta}. \tag{17}$$

The Kuhn-Tucker's loading-unloading consistency conditions demands

$$\frac{\partial\mathcal{L}}{\partial\Delta\gamma} = 0 \qquad \Rightarrow \qquad \Delta\gamma \geqslant 0; \quad \phi \leqslant 0; \quad \Delta\gamma\,\phi = 0. \tag{18}$$

The plastic strain increment and material flow direction tensor at yield is governed by the gradient of the plastic flow potential resulting from the equation (16). Mathematically, constitutive relationship for elastoplasticity can be established using both associated as well as non-associated flow rule.

2.3. Associated flow rule

Associated flow rule implies that the plastic flow develops along the normal to the predicted yield surface. The projected flow tensor as the gradient of yield

Please cite this article as:
V. Laheri, P. Hao, F.A. Gilabert.
"Efficient non-iterative modelling of pressure-dependent plasticity using paraboloidal yield criterion".
International Journal of Mechanical Sciences (2021), DOI: https://doi.org/10.1016/j.ijmecsci.2021.106988
Received: 18 Jul 2021, Revised: 25 Oct 2021, Accepted: 5 Dec 2021.

surface as inferred from the plastic strain evolution relation (16) is expressed as

$$\mathbf{N} = \frac{\partial \phi^{tr}}{\partial \boldsymbol{\sigma}^{tr} = 3\boldsymbol{\sigma}^{tr\prime} - (\sigma_t - \sigma_c)\ \mathbf{I}}, \tag{19}$$

where the superscript "tr" stands for trial stress based on the prediction of total strain comprising elastic part. The surface normal is typically, a dimensionless direction tensor along which the predicted stress is mapped on the yield surface. Therefore, the relation deduced in equation (19), is required to be normalised by an effective scalar quantity $\hat{n}$, given by

$$\hat{n} = \|\mathbf{N}\| = \sqrt{6\overline{\sigma}^{tr\,2} + 3\,(\sigma_t - \sigma_c)^2}, \tag{20}$$

for the formulation of yield surface normal

$$\boldsymbol{\eta} = \frac{\mathbf{N}}{\hat{n}} = \frac{3\boldsymbol{\sigma}^{tr\prime} - (\sigma_t - \sigma_c)\ \mathbf{I}}{\hat{n}}. \tag{21}$$

Associatively splitting the expression for flow normal (21) results in the deviatoric $\boldsymbol{\eta}' = (3/\hat{n})\,\boldsymbol{\sigma}^{tr\prime}$ and the hydrostatic $\boldsymbol{\eta}^K = -\left[(\sigma_t - \sigma_c)/\hat{n}\right]\mathbf{I}$ parts.

Plastic strain increment

From the stress update using radial return mapping algorithm (exhaustively documented in the algorithm 1) to determine the plastic strain increment, we arrive at

$$\begin{aligned}
\boldsymbol{\sigma}_{n+1} &= \boldsymbol{\sigma}^{tr}_{n+1} - \mathbb{C}^e : \Delta\boldsymbol{\varepsilon}^p \qquad (22)\\
&= \boldsymbol{\sigma}^{tr}_{n+1} - \left(2\mu\mathbb{P} + \kappa\bar{\mathbb{I}}\right) : (\Delta\gamma\boldsymbol{\eta})\\
&= \boldsymbol{\sigma}^{tr}_{n+1} - \Delta\gamma\left(2\mu\boldsymbol{\eta}' + 3\kappa\boldsymbol{\eta}^K\right)\\
\boldsymbol{\sigma}_{n+1} &= \boldsymbol{\sigma}^{tr}_{n+1} - \Delta\gamma\left[2\mu\frac{3}{\hat{n}}\boldsymbol{\sigma}^{tr\prime} - 3\kappa\frac{(\sigma_t - \sigma_c)}{\hat{n}}\mathbf{I}\right], \qquad (23)
\end{aligned}$$

where the subscript "$n+1$" represents the history count. For brevity, the latest counter is dropped.

The above mapping stress relation can be further decomposed into its devi-

Please cite this article as:
V. Laheri, P. Hao, F.A. Gilabert.
"Efficient non-iterative modelling of pressure-dependent plasticity using paraboloidal yield criterion".
International Journal of Mechanical Sciences (2021), DOI: https://doi.org/10.1016/j.ijmecsci.2021.106988
Received: 18 Jul 2021, Revised: 25 Oct 2021, Accepted: 5 Dec 2021.

atoric and volumetric components. Subsequently, both the components can be further devised to represent the associatively split terms of yield criterion

$$\begin{aligned}
\boldsymbol{\sigma}' &= \boldsymbol{\sigma}^{tr\prime} - \Delta\gamma\,\frac{6\mu}{\hat{n}}\boldsymbol{\sigma}^{tr\prime} \\
\frac{3}{2}\boldsymbol{\sigma}' : \boldsymbol{\sigma}' &= \left(1 - \frac{6\mu}{\hat{n}}\,\Delta\gamma\right)^2 \frac{3}{2}\boldsymbol{\sigma}^{tr\prime} : \boldsymbol{\sigma}^{tr\prime} \\
\overline{\sigma}^2 &= \left(1 - \frac{6\mu}{\hat{n}}\,\Delta\gamma\right)^2 \overline{\sigma}^{tr\,2} \\
\overline{\sigma}^2 &= \left(1 - \frac{12\mu}{\hat{n}}\,\Delta\gamma + \frac{36\mu^2}{\hat{n}^2}\,\Delta\gamma^2\right)\overline{\sigma}^{tr\,2}
\end{aligned} \tag{24}$$

and

$$\begin{aligned}
\boldsymbol{\sigma}^K &= \boldsymbol{\sigma}^{tr\,K} + \Delta\gamma\, 3\kappa\frac{(\sigma_t - \sigma_c)}{\hat{n}}\,\mathbf{I} \\
\boldsymbol{\sigma} : \mathbf{I} &= \boldsymbol{\sigma}^{tr} : \mathbf{I} + 9\kappa\frac{(\sigma_t - \sigma_c)}{\hat{n}}\Delta\gamma \\
(\sigma_t - \sigma_c)\, I_1 &= (\sigma_t - \sigma_c)\, I_1^{tr} + 9\kappa\frac{(\sigma_t - \sigma_c)^2}{\hat{n}}\,\Delta\gamma.
\end{aligned} \tag{25}$$

Upon rearranging the above relations of stress invariants (24) and (25) in order to represent the yield function on the left hand-side of the equation, we get

$$\begin{aligned}
\overline{\sigma}^2 - (\sigma_t - \sigma_c)\, I_1 - \sigma_t\,\sigma_c &= \left(1 - \frac{12\mu}{\hat{n}}\,\Delta\gamma + \frac{36\mu^2}{\hat{n}^2}\,\Delta\gamma^2\right)\overline{\sigma}^{tr\,2} \\
&- (\sigma_t - \sigma_c)\, I_1^{tr} - 9\kappa\frac{(\sigma_t - \sigma_c)^2}{\hat{n}}\,\Delta\gamma - (\sigma_t + h\Delta\overline{\epsilon}^p)\,(\sigma_c + h\Delta\overline{\epsilon}^p)\,.
\end{aligned} \tag{26}$$

Substituting the deviatoric part of the flow normal from equation (21) in the plastic strain evolution relation (16), the equivalent plastic strain relation (3) can be further simplified to

$$\Delta\overline{\epsilon}^p = \sqrt{\Delta\gamma^2\left(\tfrac{2}{3}\boldsymbol{\eta}' : \boldsymbol{\eta}'\right)} = 2\frac{\overline{\sigma}^{tr}}{\hat{n}}\,\Delta\gamma. \tag{27}$$

Please cite this article as:
V. Laheri, P. Hao, F.A. Gilabert.
"Efficient non-iterative modelling of pressure-dependent plasticity using paraboloidal yield criterion".
International Journal of Mechanical Sciences (2021), DOI: https://doi.org/10.1016/j.ijmecsci.2021.106988
Received: 18 Jul 2021, Revised: 25 Oct 2021, Accepted: 5 Dec 2021.

Substituting relation (27) in (26) yields,

$$\begin{aligned}\phi(\Delta\gamma) = \phi^{tr} + \frac{4\overline{\sigma}^{tr\,2}}{\hat{n}^2}\left(9\mu^2 - h^2\right)\Delta\gamma^2 \\ - \frac{12\mu\overline{\sigma}^{tr\,2} + 9\kappa\left(\sigma_t - \sigma_c\right)^2 + 2h\left(\sigma_t + \sigma_c\right)\overline{\sigma}^{tr}}{\hat{n}}\Delta\gamma.\end{aligned} \tag{28}$$

The return mapping of the plastic strain on the yield surface allows the elimination of the corresponding amount of plastic stress, thereby causing to fulfil the equation (28), i.e., $\phi(\Delta\gamma) = 0$

$$\frac{4\overline{\sigma}^{tr\,2}}{\hat{n}^2}\left(9\mu^2 - h^2\right)\Delta\gamma^2 - \frac{12\mu\overline{\sigma}^{tr\,2} + 9\kappa\left(\sigma_t - \sigma_c\right)^2 + 2h\left(\sigma_t + \sigma_c\right)\overline{\sigma}^{tr}}{\hat{n}}\Delta\gamma + \phi^{tr} = 0 \tag{29}$$

Interestingly, the equation (29) above is a quadratic equation of the variable $\Delta\gamma$, the absolute solution of which is readily given by,

$$\Delta\gamma_{1,2} = \frac{-b \pm \sqrt{b^2 - 4ac}}{2a}, \tag{30}$$

where the coefficients, a, b, and c of the variable $\Delta\gamma$ from the equation (29) are

$$a = \frac{4\overline{\sigma}^{tr\,2}}{\hat{n}^2}\left(9\mu^2 - h^2\right) \tag{31}$$

$$b = -\frac{12\mu\overline{\sigma}^{tr\,2} + 9\kappa\left(\sigma_t - \sigma_c\right)^2 + 2h\left(\sigma_t + \sigma_c\right)\overline{\sigma}^{tr}}{\hat{n}} \tag{32}$$

$$c = \phi^{tr} = \overline{\sigma}^{tr\,2} - \left(\sigma_t - \sigma_c\right) I_1^{tr} - \sigma_t\,\sigma_c. \tag{33}$$

Care must be taken for obtaining real solutions of the increment of plastic strain multiplier from equation (30). In case of multiple solutions, selection of an optimised value can be achieved by implementation of the classical loading-unloading conditions (18). The optimisation process is further elucidated in the subsection 3.1.

Please cite this article as:
V. Laheri, P. Hao, F.A. Gilabert.
"Efficient non-iterative modelling of pressure-dependent plasticity using paraboloidal yield criterion".
International Journal of Mechanical Sciences (2021), DOI: https://doi.org/10.1016/j.ijmecsci.2021.106988
Received: 18 Jul 2021, Revised: 25 Oct 2021, Accepted: 5 Dec 2021.

Consistent elastoplastic tangent modulus

The consistent elastoplastic tangent modulus is the tensorial differentiation of updated stress (equation (22)) from the radial return mapping derived as follows

$$\begin{aligned}\mathbb{C}^{ep} = \frac{\partial \boldsymbol{\sigma}}{\partial \boldsymbol{\varepsilon}^{e}} &= \frac{\partial \boldsymbol{\sigma}^{tr}}{\partial \boldsymbol{\varepsilon}^{tr,e}} - \{\mathbb{C}^{e} : \boldsymbol{\eta}\} \otimes \frac{\partial \Delta\gamma}{\partial \boldsymbol{\varepsilon}^{e,tr}} - \Delta\gamma \frac{\partial \{\mathbb{C}^{e} : \boldsymbol{\eta}\}}{\partial \boldsymbol{\varepsilon}^{e,tr}} \\ &= \mathbb{C}^{e} - \{\mathbb{C}^{e} : \boldsymbol{\eta}\} \otimes \frac{\partial \Delta\gamma}{\partial \boldsymbol{\varepsilon}^{e,tr}} - \Delta\gamma \frac{\partial \{\mathbb{C}^{e} : \boldsymbol{\eta}\}}{\partial \boldsymbol{\varepsilon}^{e,tr}} \end{aligned} \tag{34}$$

where "⊗" operator is a dyadic product operator.

The partial differentiations of the terms in elastoplastic tangent operator (34) is derived as

$$\frac{\partial \{\mathbb{C}^{e} : \boldsymbol{\eta}\}}{\partial \boldsymbol{\varepsilon}^{e,tr}} = \frac{12\mu^2}{\hat{n}} \left(\mathbb{P} - \boldsymbol{\eta}' \otimes \boldsymbol{\eta}'\right) - \frac{3}{\hat{n}} \left(2\mu\boldsymbol{\eta}' \otimes 3\kappa\boldsymbol{\eta}^{K}\right) \tag{35}$$

and

$$\frac{\partial \Delta\gamma}{\partial \boldsymbol{\varepsilon}^{e,tr}} = \frac{1}{2a} \left\{ b_{,\boldsymbol{\varepsilon}} \pm \frac{b\,(b_{,\boldsymbol{\varepsilon}}) - 2\left[(a_{,\boldsymbol{\varepsilon}})\,c + a\,(c_{,\boldsymbol{\varepsilon}})\right]}{\sqrt{b^2 - 4ac}} \right\} - \frac{\Delta\gamma}{a} a_{,\boldsymbol{\varepsilon}}\,. \tag{36}$$

The differentials of the coefficients can be expanded as

$$a_{,\boldsymbol{\varepsilon}} = \frac{\partial a}{\partial \boldsymbol{\varepsilon}^{e,tr}} = \frac{72\mu}{\hat{n}^2} \left(9\mu^2 - h^2\right) (\sigma_t - \sigma_c)^2\, \boldsymbol{\sigma}^{tr\prime} \tag{37}$$

$$b_{,\boldsymbol{\varepsilon}} = \frac{\partial b}{\partial \boldsymbol{\varepsilon}^{e,tr}} = -\frac{6\mu}{\hat{n}} \left[12\mu + h\frac{(\sigma_t + \sigma_c)}{\overline{\sigma}^{tr}} + 3\frac{b}{\hat{n}}\right] \boldsymbol{\sigma}^{tr\prime} \tag{38}$$

$$c_{,\boldsymbol{\varepsilon}} = \frac{\partial c}{\partial \boldsymbol{\varepsilon}^{e,tr}} = 6\mu\boldsymbol{\sigma}^{tr\prime} - 3\kappa(\sigma_t - \sigma_c)\mathbf{I}, \tag{39}$$

where the differentials of invariants with respect to the strain tensor is generally expressed as,

$$\frac{\partial\, \overline{\sigma}}{\partial \boldsymbol{\varepsilon}} = \frac{\partial \left[\frac{3}{2}\,(2\mu\boldsymbol{\varepsilon}' : 2\mu\boldsymbol{\varepsilon}')\right]^{1/2}}{\partial \boldsymbol{\varepsilon}} = \frac{3\mu}{\overline{\sigma}}\boldsymbol{\sigma}' \tag{40}$$

$$\frac{\partial\, I_1}{\partial \boldsymbol{\varepsilon}} = \frac{\partial \left[3\kappa(\boldsymbol{\varepsilon} : \mathbf{I})\right]}{\partial \boldsymbol{\varepsilon}} = 3\kappa\mathbf{I}. \tag{41}$$

Please cite this article as:
V. Laheri, P. Hao, F.A. Gilabert.
"Efficient non-iterative modelling of pressure-dependent plasticity using paraboloidal yield criterion".
International Journal of Mechanical Sciences (2021), DOI: https://doi.org/10.1016/j.ijmecsci.2021.106988
Received: 18 Jul 2021, Revised: 25 Oct 2021, Accepted: 5 Dec 2021.

2.4. *Non-associated flow rule*

In a non-associated flow, the direction tensor of the plastic strain rate follows the tangent of an alternative flow potential function instead of the yield surface. Following the deductions of Kolling et. al. [29], the general non-associated flow potential is proposed as

$$g = \overline{\sigma}^2 + \frac{\alpha_0}{9} I_1^2, \tag{42}$$

where the coefficient α_0 is associated to the volumetric part of plastic flow and is dependent upon the plastic Poisson's ratio ν^p. Conceptualised by Charalambides and Dean [11], ν^p varies with plastic hardening progression. Duncan et. al. [17] showed that the value of ν^p ranges from 0.3 to 0.5 as an indicator to the volume increase during plastic yielding. The pressure-dependent coefficient α_0 as a function of ν^p is defined as

$$\alpha_0\left(\nu^p\right) = \frac{9}{2}\left(\frac{1-2\nu^p}{1+\nu^p}\right). \tag{43}$$

Using the flow potential function (42), the plasticity flow rule for determination of the plastic strain increment is given by

$$\Delta\boldsymbol{\varepsilon}^p = \Delta\gamma \frac{\partial g}{\partial \boldsymbol{\sigma}}. \tag{44}$$

The flow normal is redefined as the tangent to the predicted flow potential $\mathbf{N} = \partial g^{tr}/\partial \boldsymbol{\sigma}^{tr}$ as follows

$$\mathbf{N} = \frac{\partial g^{tr}}{\partial \boldsymbol{\sigma}^{tr} = 3\boldsymbol{\sigma}^{tr\prime} + \frac{2}{9}\alpha_0 I_1^{tr}\mathbf{I}}. \tag{45}$$

Applying the normalisation treatment with its effective scalar quantity $\hat{n} = \sqrt{6\overline{\sigma}^{tr2} + 3\left(\frac{2}{9}\alpha_0 I_1^{tr}\right)^2}$, the flow normal can be reformulated with its deviatoric and hydrostatic split as

$$\boldsymbol{\eta} = \boldsymbol{\eta}' + \boldsymbol{\eta}^K = \frac{3\boldsymbol{\sigma}^{tr\prime} + \frac{2}{9}\alpha_0 I_1^{tr}\mathbf{I}}{\hat{n}}. \tag{46}$$

15

Please cite this article as:
V. Laheri, P. Hao, F.A. Gilabert.
"Efficient non-iterative modelling of pressure-dependent plasticity using paraboloidal yield criterion".
International Journal of Mechanical Sciences (2021), DOI: https://doi.org/10.1016/j.ijmecsci.2021.106988
Received: 18 Jul 2021, Revised: 25 Oct 2021, Accepted: 5 Dec 2021.

Plastic strain increment

The stress update using radial return mapping algorithm to determine the plastic strain increment, we get

$$\begin{aligned}\boldsymbol{\sigma}_{n+1} &= \boldsymbol{\sigma}^{tr}_{n+1} - \mathbb{C}^e : \Delta\boldsymbol{\varepsilon}^p \\ \boldsymbol{\sigma}_{n+1} &= \boldsymbol{\sigma}^{tr}_{n+1} - \Delta\gamma\left(2\mu\frac{3}{\hat{n}}\,\boldsymbol{\sigma}^{tr\prime} + 3\kappa\frac{2}{9}\frac{\alpha_0}{\hat{n}}\,I_1^{tr}\,\mathbf{I}\right).\end{aligned} \tag{47}$$

Decomposing the above stress tensor again into its deviatoric and volumetric components and formulating them in terms of yield criterion, we get a similar relation of equivalent stress like in associated flow rule but a dissimilar relation for the 1st stress invariant

$$\overline{\sigma}^2 = \left(1 - \frac{12\mu}{\hat{n}}\,\Delta\gamma + \frac{36\mu^2}{\hat{n}^2}\,\Delta\gamma\right)\overline{\sigma}^{tr\,2}, \qquad \text{from (24)}$$

and

$$\begin{aligned}\boldsymbol{\sigma}^K &= \boldsymbol{\sigma}^{tr\,K} - \Delta\gamma\,\frac{2}{3}\frac{\kappa\,\alpha_0}{\hat{n}}\,I_1\,\mathbf{I} \\ (\sigma_t - \sigma_c)\,I_1 &= (\sigma_t - \sigma_c)\,I_1^{tr} - 2\frac{\kappa\,\alpha_0}{\hat{n}}\,(\sigma_t - \sigma_c)\,I_1^{tr}\,\Delta\gamma.\end{aligned} \tag{48}$$

Similar rearranging technique to represent the yield function on the left hand-side of the equation can be reapplied to the obtained relations of invariants in (24) and (48), where it yields

$$\begin{aligned}\overline{\sigma}^2 - (\sigma_t - \sigma_c)\,I_1 - \sigma_t\,\sigma_c &= \left(1 - \frac{12\mu}{\hat{n}}\,\Delta\gamma + \frac{36\mu^2}{\hat{n}^2}\,\Delta\gamma\right)\overline{\sigma}^{tr\,2} \\ &\quad - (\sigma_t - \sigma_c)\,I_1^{tr} + 2\frac{\kappa\,\alpha_0}{\hat{n}}\,(\sigma_t - \sigma_c)\,I_1^{tr}\,\Delta\gamma - (\sigma_t + h\Delta\overline{\epsilon}^p)\,(\sigma_c + h\Delta\overline{\epsilon}^p)\,.\end{aligned} \tag{49}$$

Please cite this article as:
V. Laheri, P. Hao, F.A. Gilabert.
"Efficient non-iterative modelling of pressure-dependent plasticity using paraboloidal yield criterion".
International Journal of Mechanical Sciences (2021), DOI: https://doi.org/10.1016/j.ijmecsci.2021.106988
Received: 18 Jul 2021, Revised: 25 Oct 2021, Accepted: 5 Dec 2021.

Reusing the relation (27) for equivalent plastic strain in (49), we get

$$\phi(\Delta\gamma) = \phi^{tr} + \frac{4\overline{\sigma}^{tr\,2}}{\hat{n}^2}\left(9\mu^2 - h^2\right)\Delta\gamma^2 - \frac{12\mu\overline{\sigma}^{tr\,2} - 2\kappa\,\alpha_0\,(\sigma_t - \sigma_c)\,I_1^{tr} + 2h\,(\sigma_t + \sigma_c)\,\overline{\sigma}^{tr}}{\hat{n}}\Delta\gamma. \tag{50}$$

For return mapping of the plastic strain on the yield surface, fulfilment of the equation (50) results in another quadratic equation of plastic strain increment variable $\Delta\gamma$, as follows

$$\frac{4\overline{\sigma}^{tr\,2}}{\hat{n}^2}\left(9\mu^2 - h^2\right)\Delta\gamma^2 - \frac{12\mu\overline{\sigma}^{tr\,2} - 2\kappa\,\alpha_0\,(\sigma_t - \sigma_c)\,I_1^{tr} + 2h\,(\sigma_t + \sigma_c)\,\overline{\sigma}^{tr}}{\hat{n}}\Delta\gamma + \phi^{tr} = 0. \tag{51}$$

The absolute solution once more relies on the roots of quadratic equation $\Delta\gamma$ as the variable. It is given by the same quadratic roots as in (30) with the same coefficient c as in (33). The coefficient a is apparently similar but has a different $\hat{n}$ in denominator as compared to (31) in the associated flow. Besides, the coefficients b also differs from (32) because of the incorporation of an additional pressure-dependent term as follows

$$b = -\frac{12\mu\overline{\sigma}^{tr\,2} - 2\kappa\,\alpha_0\,(\sigma_t - \sigma_c)\,I_1^{tr} + 2h\,(\sigma_t + \sigma_c)\,\overline{\sigma}^{tr}}{\hat{n}}. \tag{52}$$

Consistent elastoplastic tangent modulus

The consistent elastoplastic tangent modulus is also expressed similarly as in (34)

$$\mathbb{C}^{ep} = \mathbb{C}^{e} - \{\mathbb{C}^{e} : \boldsymbol{\eta}\} \otimes \frac{\partial\Delta\gamma}{\partial\boldsymbol{\varepsilon}^{e,tr}} - \Delta\gamma\,\frac{\partial\,\{\mathbb{C}^{e} : \boldsymbol{\eta}\}}{\partial\boldsymbol{\varepsilon}^{e,tr}}. \qquad \text{from (34)}$$

The partial differentiation of $\Delta\gamma$ and the coefficient c in elastoplastic tangent operator remains unchanged as expressed in equations (36) and (39), respectively.

Please cite this article as:
V. Laheri, P. Hao, F.A. Gilabert.
"Efficient non-iterative modelling of pressure-dependent plasticity using paraboloidal yield criterion".
International Journal of Mechanical Sciences (2021), DOI: https://doi.org/10.1016/j.ijmecsci.2021.106988
Received: 18 Jul 2021, Revised: 25 Oct 2021, Accepted: 5 Dec 2021.

Owing to the the different denominator $\hat{n}$, its partial differentiation is deduced as

$$a_{,\boldsymbol{\varepsilon}} = \frac{\partial a}{\partial \boldsymbol{\varepsilon}^{e,tr}} = \frac{32}{9}\frac{\alpha_0^2}{\hat{n}^4} I_1^{tr} \left(9\mu^2 - h^2\right) \left(\mu\, I_1^{tr} \boldsymbol{\sigma}^{tr\prime} - \kappa\, \overline{\sigma}^{tr^2}\, \mathbf{I}\right) \tag{53}$$

The term $\mathbb{C}^e : \boldsymbol{\eta}$ and the coefficient b (52) contains an additional pressure-dependent part and its partial derivative with respect to the predicted elastic strain tensor $\boldsymbol{\varepsilon}^{e,tr}$ can be expanded as

$$\begin{aligned}\frac{\partial \left\{\mathbb{C}^e : \boldsymbol{\eta}\right\}}{\partial \boldsymbol{\varepsilon}^{e,tr}} &= \frac{\partial \left\{\dfrac{6\mu}{\hat{n}}\boldsymbol{\sigma}^{tr\prime} + \dfrac{2}{3}\dfrac{\kappa\alpha_0}{\hat{n}} I_1\, \mathbf{I}\right\}}{\partial \boldsymbol{\varepsilon}^{e,tr}} \\ &= \frac{1}{\hat{n}}\left\{12\mu^2\left(\mathbb{P} - \boldsymbol{\eta}'\otimes\boldsymbol{\eta}'\right) - 3\left(3\kappa\,\boldsymbol{\eta}^K \otimes 2\mu\,\boldsymbol{\eta}'\right)\right. \\ &\quad \left. + \frac{2}{9}\alpha_0\left[(3\kappa)^2\bar{\mathbb{I}} - 3\left(2\mu\,\boldsymbol{\eta}'\otimes 3\kappa\,\boldsymbol{\eta}^K\right) - 3\left(3\kappa\,\boldsymbol{\eta}^K \otimes 3\kappa\,\boldsymbol{\eta}^K\right)\right]\right\}\end{aligned} \tag{54}$$

and

$$b_{,\boldsymbol{\varepsilon}} = \frac{\partial b}{\partial \boldsymbol{\varepsilon}^{e,tr}} = -\frac{6\mu}{\hat{n}}\left[12\mu + h\frac{(\sigma_t + \sigma_c)}{\overline{\sigma}^{tr}} + 3\frac{b}{\hat{n}}\right]\boldsymbol{\sigma}^{tr\prime} - 2\kappa\frac{\alpha_0}{\hat{n}}\left[b\boldsymbol{\eta}^K - 3\kappa(\sigma_t - \sigma_c)\mathbf{I}\right]. \tag{55}$$

3. Numerical implementation

The implicit elastic predictor method is a conventional approach to map the excessively predicted stress along the normal to the yield surface. In principle, the algorithm is manoeuvred to determine and eliminate the strain increment due to plastic yielding from the total strain increment, resulting in the overall elastic effect. Its implementation is featured in algorithm 1 for the finite element computation, provided the state variables of the evolution are recorded.

The following subsection 3.1 is dedicated to explain and draw a comparison of the computational schemes for the evolution of plastic strain, $\Delta\gamma$ stated in step 7 of the algorithm 1 using the proposed mathematical model and the one postulated by Melro [32].

Please cite this article as:
V. Laheri, P. Hao, F.A. Gilabert.
"Efficient non-iterative modelling of pressure-dependent plasticity using paraboloidal yield criterion".
International Journal of Mechanical Sciences (2021), DOI: https://doi.org/10.1016/j.ijmecsci.2021.106988
Received: 18 Jul 2021, Revised: 25 Oct 2021, Accepted: 5 Dec 2021.

Algorithm 1: Implicit elastic predictor method (radial return mapping algorithm) implementation.

▶ Get stress state and strain increment tensors @ t_n:

1 $\quad \boldsymbol{\sigma}_n \leftarrow$ `stress`

2 $\quad \Delta\boldsymbol{\varepsilon} \leftarrow$ `dstran`

▶ Elastic predictor:

3 $\quad \mathbb{C}^e = 2\mu\mathbb{P} + \kappa\bar{\mathbb{I}}$

4 $\quad \boldsymbol{\sigma}^{tr}_{n+1} = \boldsymbol{\sigma}_n + \mathbb{C}^e : \Delta\boldsymbol{\varepsilon} = \boldsymbol{\sigma}_n + 2\mu\,\Delta\boldsymbol{\varepsilon}' + 3\kappa\,\Delta\boldsymbol{\varepsilon}^K$

▶ Determine if actively yielding:

5 **if** $\left(\phi^{tr}(\boldsymbol{\sigma}^{tr}) > \epsilon_{tol}\right)$ **then**

6 $\quad$ ▹ Compute: $\boldsymbol{\eta} = \dfrac{\partial\,\phi^{tr}}{\partial\,\boldsymbol{\sigma}^{tr}}$

7 $\quad$ ▹ Compute: $\Delta\gamma$

8 $\quad$ ▹ Compute: $\Delta\boldsymbol{\varepsilon}^p = \Delta\gamma\boldsymbol{\eta}$

$\quad$ ▹ **Result:**

9 $\quad\quad \boldsymbol{\sigma}_{n+1} \leftarrow \boldsymbol{\sigma}^{tr}_{n+1} - \mathbb{C}^e : \Delta\boldsymbol{\varepsilon}^p$

10 $\quad\quad \mathbb{C}_{n+1} \leftarrow \mathbb{C}^{ep}$

11 **else**

$\quad$ ▹ **Result:**

12 $\quad\quad \boldsymbol{\sigma}_{n+1} \leftarrow \boldsymbol{\sigma}^{tr}_{n+1}$

13 $\quad\quad \mathbb{C}_{n+1} \leftarrow \mathbb{C}^e$

14 **return**

3.1. Computational scheme

The elastic predictor approach ensuing radial return algorithm is an empirically heuristic method for numerical modelling of elastoplasticity. However, the computation of the parameters of elastoplastic equations varies by the mathematics developed.

A school of thought [2, 3, 20, 33–35, 50, 54–56] following the works of Melro [32] employs Newton-Raphson's iterative numerical scheme to solve the non-linear system of equations and determine $\Delta\gamma$ for paraboloidal yielding under non-associated plastic flow computed using the algorithm 2. The variables h_c and h_t in the statements 10 and 11 of the algorithm 2 refer to the hardening in compression and tension, respectively. Hardening is considered to be a function of equivalent plastic strain and provided piecewise [34].

Please cite this article as:
V. Laheri, P. Hao, F.A. Gilabert.
"Efficient non-iterative modelling of pressure-dependent plasticity using paraboloidal yield criterion".
International Journal of Mechanical Sciences (2021), DOI: https://doi.org/10.1016/j.ijmecsci.2021.106988
Received: 18 Jul 2021, Revised: 25 Oct 2021, Accepted: 5 Dec 2021.

The convergence rate of the iterative scheme for the approximation of $\Delta\gamma$ is quadratic but inexact, thus adding to a cumulative error in the computation of stress and consistent tangent modulus. Sepasdar and Shakiba [46] determined that the cohesive zone models also suffer from convergence difficulty due to the iterative scheme and proposed methods to modify the starting point and overcome it. The numerical scheme functions on the definition of an initial guess of plastic strain increment multiplier $\Delta\gamma^0$ (refer 1). Volmer *et al.* [57] identified the convergence problem inherent with the constitutive model dependent on iterative and perturbation schemes and discusses the techniques to improve initial guess of the Newton-Raphson scheme. Order of magnitude of $\Delta\gamma^0$ plays a pivotal role in the rate at which the convergent solution of the yield function is determined. The scheme also relies on the exact definition of the associated residual function $\partial\phi/\partial\,\Delta\gamma$, the iterative computation of which renders it a tedious endeavour.

Additionally, if the iterative scheme does not yield a value within the tolerance, i.e., if $|\Delta\gamma^{(i+1)} - \Delta\gamma^{(i)}| > \epsilon_{tol}$ in an arbitrarily limited number of iterations n_{iter}, the computation process demands improving $\Delta\gamma^{(0)}$. It further repeats the iterative scheme until it churns out a value deterministic of plastic strain increment multiplier $\Delta\gamma$. The section of this algorithm emphasising the improvement of $\Delta\gamma^{(0)}$ is, therefore, an iterative process within itself, whereby the iterative steps geometrically progress to $n_{iter} \times n_{fail}$. Moreover, might the improvement faculty of the algorithm fails within a stipulated number of failed attempts, n_{fail}, the algorithm necessitates restarting the entire computation process with a new initial guess, $\Delta\gamma^{(0)}$ which shall be smaller than the previously initialised value. It causes the process to run unconditionally infinite times.

With the mathematical model proposed in this paper, the plastic multiplier for determining plastic strain increment follows a direct computation as the root of a quadratic equation (refer equation (30)). Further processing of two roots employs the classical Kuhn-Tucker's loading-unloading conditions (refer equation (18)) as described in the algorithm 3.

The proposed algorithm qualifies to eliminate the iterative scheme, making the process computationally frugal. The robustness of the proposed model is higher as the solution of the non-linear equation for determining the plastic strain

Please cite this article as:
V. Laheri, P. Hao, F.A. Gilabert.
"Efficient non-iterative modelling of pressure-dependent plasticity using paraboloidal yield criterion".
International Journal of Mechanical Sciences (2021), DOI: https://doi.org/10.1016/j.ijmecsci.2021.106988
Received: 18 Jul 2021, Revised: 25 Oct 2021, Accepted: 5 Dec 2021.

Algorithm 2: Plastic strain increment multiplier, $\Delta\gamma$ computation used in [32].

▷ Set initial guess: $\Delta\gamma^{(0)} = 10^{-8}$

▷ Initialise fail counter: $i_{fail} = 0$

► Newton-Raphson iterative scheme:

▷ Initialise iteration counter: $i = 0$

while $(i \leqslant n_{iter})$ **do**

▷ Compute:

$\zeta_s = 1 + 6\mu\,\Delta\gamma^{(i)}$ /* FLOPS = 3 */

$\zeta_p = 1 + 2\kappa\,\alpha_0\,\Delta\gamma^{(i)}$ /* FLOPS = 4 */

$A = \dfrac{18}{\zeta_s^2} J_2^{tr} + \dfrac{4\alpha_0^2}{27\zeta_p^2} \left(I_1^{tr}\right)^2$ /* FLOPS =11 */

▷ Increment of equivalent plastic strain:

$\Delta\overline{\epsilon}^p = \sqrt{\dfrac{A}{1 + 2\left(\nu^p\right)^2}}\,\Delta\gamma^{(i)}$ /* FLOPS = 6 */

▷ Hardening variables:

$$\frac{\partial\,\Delta\overline{\epsilon}^p}{\partial\,\Delta\gamma} = \sqrt{\frac{1}{1 + 2\left(\nu^p\right)^2}} \left[\sqrt{A} - \frac{\Delta\gamma}{2\sqrt{A}} \left(\frac{216\mu}{\zeta_s^3} J_2^{tr} + \frac{16\kappa\,\alpha_0}{27\zeta_p^3} I_1^{tr}\right)\right]$$

/* FLOPS =23 */

$\dfrac{\partial\,\sigma_c(\Delta\overline{\epsilon}^p)}{\partial\,\Delta\gamma} = h_c \dfrac{\partial\,\Delta\overline{\epsilon}^p}{\partial\,\Delta\gamma}$ /* FLOPS = 2 */

$\dfrac{\partial\,\sigma_t(\Delta\overline{\epsilon}^p)}{\partial\,\Delta\gamma} = h_t \dfrac{\partial\,\Delta\overline{\epsilon}^p}{\partial\,\Delta\gamma}$ /* FLOPS = 2 */

▷ Residual derivative:

$$\frac{\partial\phi}{\partial\,\Delta\gamma} = \frac{2}{\zeta_p} I_1^{tr} \left(\frac{\partial\sigma_c}{\partial\,\Delta\gamma} - \frac{\partial\sigma_t}{\partial\,\Delta\gamma}\right) + \frac{4\kappa\,\alpha_0}{\zeta_p^2} I_1^{tr}\,(\sigma_t - \sigma_c) - \frac{72\mu}{\zeta_s^3} J_2^{tr} - 2\left(\sigma_c \frac{\partial\sigma_t}{\partial\,\Delta\gamma} + \sigma_t \frac{\partial\sigma_c}{\partial\,\Delta\gamma}\right)$$

/* FLOPS =22 */

▷ New estimate:

$\Delta\gamma^{(i+1)} = \Delta\gamma^{(i)} - \frac{\phi}{\partial\phi\,/\,\partial\,\Delta\gamma}$ /* FLOPS = 2 */

▷ Check for convergence:

if $\left(\phi(\Delta\gamma^{(i+1)}) \leqslant \epsilon_{tol}\right)$ **then** /* FLOPS = 1 */

return: $\Delta\gamma_{n+1} = \Delta\gamma^{(i+1)}$

▷ Increment iteration counter: $i = i + 1$

Please cite this article as:
V. Laheri, P. Hao, F.A. Gilabert.
"Efficient non-iterative modelling of pressure-dependent plasticity using paraboloidal yield criterion".
International Journal of Mechanical Sciences (2021), DOI: https://doi.org/10.1016/j.ijmecsci.2021.106988
Received: 18 Jul 2021, Revised: 25 Oct 2021, Accepted: 5 Dec 2021.

► Improve initial guess:
if $(i > n_{iter})$ **then** /* FLOPS = 1 */
  ▹ $i_{fail} = i_{fail} + 1$; /* FLOPS = 1 */
  ▹ $factor = 10$
  if $\left(i_{fail} \leqslant n_{fail}\right)$ **then** /* FLOPS = 1 */
    ▹ $\Delta\gamma^{(0)} = \Delta\gamma^{(0)} \times (factor)^{(i_{fail})}$; /* FLOPS = 2 */
  else
    ▹ Reset initial guess: $\Delta\gamma^{(0)} = (< \Delta\gamma^{(0)}$ at **1**) ; /* FLOPS = 1 */
  ▹ GOTO **3**.

increment multiplier is absolute and algorithmically efficient with no iterative looping. The approach straightforwardly relies on classical loading-unloading conditions to determine a unique value of plastic strain increment and is thus, highly accurate.

There could be no valid measure for ascertaining the robustness of a mathematical model to be employed in a finite element analysis than methodically examining the residual errors by scrutinizing the number of steps and cutbacks the simulation necessitates to complete its processing. The implicit analysis method, by virtue, inherently mandates that the converged solution is reached at every time step. In the case of non-convergence, the residual errors grow more significant than the approved tolerance. The solver system attempts to optimise the solution by further shortening the time increment dt until convergence is reached. The solver gradually catches up with the preordained maximum time increment dt_{max} in further progressions.

Besides, the algorithms 2 and 3 also presents the number of floating-point operations (FLOPS) a particular step involves for the computation of a variable. The number of FLOPS provides an overview of the computational effort of an algorithm since the intermittent computation is often required to be stored in the temporary memory of the system for easy accessibility. The number of FLOPS for calculation of the coefficients a, b and c of quadratic equation (51) in the mathematical model for non-associated plasticity proposed in this paper are 9, 15 and 6, respectively. These are unaccounted in the algorithm 3 to avoid repetition.

Please cite this article as:
V. Laheri, P. Hao, F.A. Gilabert.
"Efficient non-iterative modelling of pressure-dependent plasticity using paraboloidal yield criterion".
International Journal of Mechanical Sciences (2021), DOI: https://doi.org/10.1016/j.ijmecsci.2021.106988
Received: 18 Jul 2021, Revised: 25 Oct 2021, Accepted: 5 Dec 2021.

Algorithm 3: Plastic strain increment multiplier, $\Delta\gamma$ computation using proposed model.

▷ Get $\Delta\gamma_n \leftarrow$ `state variable`
▷ Initialise: $\Delta\gamma_{n+1} \leftarrow \Delta\gamma_n$ `// back-up value`
▷ Discriminant: $\triangle = b^2 - 4ac$ `/* FLOPS = 4 */`
► Determine if $\triangle$ is positive, for real roots:
if $(\triangle \geqslant 0)$ **then** `/* FLOPS = 1 */`
  ▷ Compute roots: $\Delta\gamma_{1,2} = \dfrac{-b \pm \sqrt{\triangle}}{2a}$ `/* FLOPS = 8 */`
  ▷ Compute function values: $\phi_{1,2} = a\,\Delta\gamma_{1,2}^2 + b\,\Delta\gamma_{1,2} + \phi^{tr}$ `/* FLOPS =10 */`
  ► Determine the root following Kuhn-Tucker's loading-unloading conditions:
  if $(\Delta\gamma_1 \geqslant 0 \quad and \quad \phi_1 \leqslant 0 \quad and \quad \Delta\gamma_1\phi_1 = 0)$ **then** `/* FLOPS = 4 */`
    Result: $\Delta\gamma_{n+1} \leftarrow \Delta\gamma_1$
  else if $(\Delta\gamma_2 \geqslant 0 \quad and \quad \phi_2 \leqslant 0 \quad and \quad \Delta\gamma_2\phi_2 = 0)$ **then** `/* FLOPS = 4 */`
    Result: $\Delta\gamma_{n+1} \leftarrow \Delta\gamma_2$
return: $\Delta\gamma_{n+1}$

In totality, the number of `FLOPS` in algorithm 3 is lesser than that in 2. On top of that, the iterative scheme augments the computational efforts multifold; at least n_{iter} times, considering the best-case scenario.

For a convergent solution, the FEM solver attempts to verify if the tangent modulus provided to it is in equilibrium to the growth of stress as a function of strain using the unconditionally stable implicit method. It accentuates the necessity of accurate formulation of the tangent modulus. The consistent elastoplastic tangent operator expressed in [32] is

$$\mathbb{C}^{ep} = v\,\mathbb{I}^{sym} + \left(w - \frac{v}{3}\right)\bar{\mathbb{I}} - x\,\boldsymbol{\sigma}' \otimes \mathbf{I} - y\,\boldsymbol{\sigma}' \otimes \boldsymbol{\sigma}' - z\,\mathbf{I} \otimes \boldsymbol{\sigma}'. \tag{56}$$

Please cite this article as:
V. Laheri, P. Hao, F.A. Gilabert.
"Efficient non-iterative modelling of pressure-dependent plasticity using paraboloidal yield criterion".
International Journal of Mechanical Sciences (2021), DOI: https://doi.org/10.1016/j.ijmecsci.2021.106988
Received: 18 Jul 2021, Revised: 25 Oct 2021, Accepted: 5 Dec 2021.

The constants v, w, x, y, and z are given by

$$\begin{aligned} v &= \frac{2\mu}{\zeta_s}, \quad w = \frac{\kappa}{\zeta_p} - \frac{4\kappa^2\alpha_0}{\eta\zeta_p^3} I_1^{tr} \left(\sigma_c - \sigma_t\right), \\ x &= \frac{36\mu\kappa}{\eta\zeta_s^2\zeta_p} \left(\sigma_c - \sigma_t\right), \quad y = \frac{72\mu^2}{\eta\zeta_s^4}, \quad z = \frac{8\mu\kappa\alpha_0}{\eta\zeta_p^2\zeta_s} I_1^{tr}, \end{aligned} \tag{57}$$

where $\eta = -\frac{\partial\phi}{\partial\Delta\gamma}$. The above relations (57) along with the recomputation of the constants ζ_s, ζ_p, and the residual derivative, $\frac{\partial\phi}{\partial\Delta\gamma}$ are based on the $\Delta\gamma$ value approximated through the iterative scheme. The constants ζ_s, ζ_p, and the residual derivative can be referred from statements 5, 6, and 12, respectively of algorithm 2. It not only involve additional computational operations through increased `FLOPS` but also accrue to the approximation error while determining the slope. Contrarily, the consistent elastoplastic tangent modulus postulated in the paper is also based on the exactly computed $\Delta\gamma$.

A detailed discussion will be presented in the next section while discussing numerical simulations for different geometrical models.

4. Numerical investigations

For numerical validation of the proposed non-iterative mathematical scheme of elastoplastic response using paraboloidal yielding, the representative radial return mapping algorithm 1 is implemented in the user material subroutine of the FEA/FEM software. The material subroutines incorporate the plastic strain multiplier computational algorithms 2 and 3. The results of the two mathematical models are analysed comparatively. As the paper focuses on simulating the elastoplastic response of epoxy polymers, the reference material parameters of a typical thermosetting plastic are used.

4.1. Data preparation

Table 3 encapsulates the typical elastoplastic material properties for epoxy resin used in the numerical simulations. Guild et. al. [23] predicted a constant value of $\nu^p = 0.32$ as the best fit for numerical analysis of epoxy polymer.

Please cite this article as:
V. Laheri, P. Hao, F.A. Gilabert.
"Efficient non-iterative modelling of pressure-dependent plasticity using paraboloidal yield criterion".
International Journal of Mechanical Sciences (2021), DOI: https://doi.org/10.1016/j.ijmecsci.2021.106988
Received: 18 Jul 2021, Revised: 25 Oct 2021, Accepted: 5 Dec 2021.

Table 3: Material properties for epoxy resin.

	Material parameters	**Values**	**Units**
Elastic:			
	E	3760	MPa
	ν	0.39	~
Plastic:			
	ν^p	0.32	~
	σ_t	29	MPa
	σ_c	67	MPa
Experimental [18]:			
	E_t	3900	MPa
	E_c	3600	MPa

It is also essential to recognise the yielding properties beforehand for the hardening moduli, h_t and h_c in tension and compression, respectively, to be computed following the evolution of yield stress (σ_y) for the corresponding plastic strain (ϵ^p). The yield stresses, σ_t and σ_c in tension and compression, respectively, at the onset of plasticity enlisted in the table 3 are also adapted from Fiedler et al. [18]. The experimentally determined elasticity modulus by Fiedler et al. [18], E_t and E_c are the accompanying individual values in tension and compression, respectively.

The plastic strains corresponding to yield stresses are extracted by the additive decomposition of strain relation

$$\epsilon^p_{\{\lambda\}} = \epsilon - \frac{\sigma}{E_{\{\lambda\}}} \qquad \forall\{\lambda\} = \begin{cases} t : \text{tension} \\ c : \text{compression} \end{cases} \tag{58}$$

where σ is the stress after yielding for the corresponding strain, ϵ and the subscript "$\{\lambda\}$" indicates the loading mode – "t", tension or "c", compression. This computation is carried out on the stress equating to the linearly spaced strain data by performing the least squares polynomial fitting using the Python®'s inherent `numpy.polyfit()` function on the stress-strain data from Fiedler et al. [18]. This exercise helps to produce equally spaced data of plastic strain correspond-

Please cite this article as:
V. Laheri, P. Hao, F.A. Gilabert.
"Efficient non-iterative modelling of pressure-dependent plasticity using paraboloidal yield criterion".
International Journal of Mechanical Sciences (2021), DOI: https://doi.org/10.1016/j.ijmecsci.2021.106988
Received: 18 Jul 2021, Revised: 25 Oct 2021, Accepted: 5 Dec 2021.

ing to yield stress for piecewise linear hardening modulus computation. This computation process is algorithmically demonstrated in the appendix 18.

The graphs for tension and compression in figure 1 show a high degree of conformance between the data computed from experimental values and the polynomially fitted values in small strain. Composite yielding is favoured by the size of test coupon [18] since increasing the dimension while retaining the shape causes ductile-brittle transition [4]. The experiments on size effects of polymer composites also conclude decreasing strength with increasing specimen size [58] because the bulk growth incorporates severe defects and voids. Therefore, the experimental compressive test data for a small cube sample is used for numerical simulation as the specimen is reasonably pristine and homogeneous throughout [18]. The curve, however, flows into the non-linearly following hyper-elastoplastic hardening after certain linearity in hardening. The data in this domain is extrapolated so that the current plasticity model with linear isotropic hardening can be employed. Therefore, the pseudo-plastic extrapolated data plot is used, generated by adding instantaneous stiffness values to Young's modulus in compression for each data point after reaching the linear asymptote. Figure 2 illustrates the instantaneous stiffness calculation procedure. Adapting from the equation (58), extrapolated plastic strain data in compression is computed as

$$\epsilon_c^p = \epsilon - \frac{\sigma}{E_c + E_{inst}}. \tag{59}$$

The tabulated array of ϵ^p and σ_y in tension and compression is ultimately supplied as user-defined plastic evolution data for isotropic strain hardening computation in their respective loading mode.

For comparing and demarcating computational efforts of the algorithms, the specifications of the machine used for running the simulations shall be standardised. For the presented work, only 1 CPU from the multi-core (Intel core i7) processor with 16 Gb RAM was used.

4.2. Single element test

A single element test is a simple means to computationally conduct a preliminary verification of the functioning and reliability of the mathematical formula-

Please cite this article as:
V. Laheri, P. Hao, F.A. Gilabert.
"Efficient non-iterative modelling of pressure-dependent plasticity using paraboloidal yield criterion".
International Journal of Mechanical Sciences (2021), DOI: https://doi.org/10.1016/j.ijmecsci.2021.106988
Received: 18 Jul 2021, Revised: 25 Oct 2021, Accepted: 5 Dec 2021.

tions for a material model. Therefore, a three-dimensional single element model is used to numerically verify with the experimental results obtained by Feidler et al. [18] under tensile, compressive, and shear loading conditions employing both the flow rules. Besides, a comparison of the iterative computational scheme (algorithm 2) and the proposed non-iterative mathematical model (algorithm 3) is also made for non-associated flow rule.

Figure 3 depicts a cube element of length 1 mm with an instance of tensile load applied on the reference point (RP). The mathematical representation of boundary conditions to be applied differently for tension/compression and simple shear loadings is tabulated below. The concentrated load applied at RP is distributed on the top surface (S_{top}) via the equation linking the two in the x and y-directions for simple shear and tension or compression, respectively. The boundary conditions are achieved by fixing the bottom surface (S_{bot}) of the cube in y-direction and the edges "E_x" and "E_z" along x and z-directions, respectively, to avoid rigid body motion under the application of tensile or compressive loading on S_{top}. On the other hand, for simple shear loading along x-direction, S_{top} is fixed along y-direction and S_{bot} is fixed along x and y-directions to avoid rigid body motion.

The graphs in figure 4 for both the flow rules conform to the elastoplastic experimental curves subjected to the three loading modes under small strain conditions. In compression mode at large strain under the provision of pseudo-plastic hardening, the numerical result for the associated flow rule shows a higher degree of conformance with the experiment compared to the non-associated flow rule. This deviation can be attributed to the hydrostatic sensitivity owing to the presence of a term $(\alpha_0/9)\, I_1^2$ for pressure correction applied in the non-associated flow potential function, g (equation (42)). Numerical modelling in shear uses the same constitutive model relying predominantly on the tensile and compressive yield stress and is indifferent to the yielding properties in shear. Therefore, the numerical results in graph show aberration from the experiment under large strain in shear.

The simulation results using the non-associated plasticity model based on the iterative scheme plotted alongside the results for non-iterative model match closely under small strain conditions. The compression and shear loading results

Please cite this article as:
V. Laheri, P. Hao, F.A. Gilabert.
"Efficient non-iterative modelling of pressure-dependent plasticity using paraboloidal yield criterion".
International Journal of Mechanical Sciences (2021), DOI: https://doi.org/10.1016/j.ijmecsci.2021.106988
Received: 18 Jul 2021, Revised: 25 Oct 2021, Accepted: 5 Dec 2021.

show fairly good concurrence until about 15% strain, but drifts on additional loading. The compression curve (figure 4b) of the mathematical model based on iterative scheme shows a discontinuity in yielding at strain above 30%. The inconsistency due to perturbations in the computations using iterative scheme in compression can be explained by studying the plots in figures 5 and 6.

Figure 5 shows plots comparing the devolution of time increment dt over the simulation time t to achieve convergence at each time-step between the implementations of iterative and non-iterative numerical schemes. Figure 6, on the other hand, represents iteration counter with the strain growth graphically. The equivalent plastic strain evolution is plotted alongside all loading modes to verify the activity in the iteration counter with the inception of plasticity. The time increment dt vs time t curves for tension (figure 5a) and shear (figure 5c) under both the numerical implementations show no sign of decrease and remain coincidental. So also, the iteration count depletes gradually over the strain growth in tension (figure 6a) and compression (figure 6c) plots. Contrastingly for compression, a downward spike is noticeable in the time increment dt plot (figure 5b) along with a gradual surge of iteration counts in plot (figure 6b). This is the region of the graph where pseudo-plasticity is applied and a distinctive perturbation is apparent for the discontinuous stress-strain region. The perturbation can be summarised as the solver's attempt to achieve localised convergence using implicit solution for the computed plastic strain increment and consistent elastoplastic tangent operator at a particular step which is inconsistent to the overall evolution of plastic strain.

Table 4: CPU time for single element test simulations.

Load	**CPU time** [s]	
	Ref. [32]	Proposed
Tension	2.0	2.3
Compression	2.5	3.0
Shear	2.5	2.6

Table 4 enlists the CPU time used by the implicit solver to complete the

Please cite this article as:
V. Laheri, P. Hao, F.A. Gilabert.
"Efficient non-iterative modelling of pressure-dependent plasticity using paraboloidal yield criterion".
International Journal of Mechanical Sciences (2021), DOI: https://doi.org/10.1016/j.ijmecsci.2021.106988
Received: 18 Jul 2021, Revised: 25 Oct 2021, Accepted: 5 Dec 2021.

simulation under three loading cases over the same time steps and initial conditions for a single element test. The algorithmic implementation employing iterative computational technique tends to consume more time as compared to the proposed non-iterative technique. With this overview, it can be concluded that the overall computational time will increase multifold with increased mesh in complex geometries.

4.3. Cylinder compression test

Compression tests of a cylinder specimen are computationally performed to test the functionality of the proposed mathematical model using realistic lab-sized geometry.

Taking advantage of the specimen's symmetry, an eighth $\left({}^{1}/_{8}\right)$ geometry is modelled as shown in the left image of figure 7 and simulated for varying element sizes to conduct the mesh convergence test. The boundary conditions are applied on the exposed planes, "PlaneA" and "PlaneB" along z and x-directions, respectively. The bottom surface, "$\mathrm{S_{bot}}$" is constrained along the y-direction. A reference point, "RP" on which the load is applied is connected to the top surface, "$\mathrm{S_{top}}$" via an equation in y-direction only such that the load is uniformly distributed on $\mathrm{S_{top}}$. The dimensions shown on a meshed instance of the geometry with element size, $\ell_{elem} = 1$ mm in the right image of figure 7 are $H = 6$ mm and $R = 6$ mm.

Figure 8 shows the comparison between the simulated and experimental results. The volume-averaged stress and strain for the model are defined using 1$^{\text{st}}$ order homogenisation, approximated as

$$\sigma_{homg} = \frac{1}{V}\int \sigma \, dV \approx \frac{\sum_{i=1}^{n_{elem}} \sigma_i \, V_i}{\sum_{i=1}^{n_{elem}} V_i} \tag{60}$$

$$\varepsilon_{homg} = \frac{1}{V}\int \varepsilon \, dV \approx \frac{\sum_{i=1}^{n_{elem}} \varepsilon_i \, V_i}{\sum_{i=1}^{n_{elem}} V_i} \tag{61}$$

Please cite this article as:
V. Laheri, P. Hao, F.A. Gilabert.
"Efficient non-iterative modelling of pressure-dependent plasticity using paraboloidal yield criterion".
International Journal of Mechanical Sciences (2021), DOI: https://doi.org/10.1016/j.ijmecsci.2021.106988
Received: 18 Jul 2021, Revised: 25 Oct 2021, Accepted: 5 Dec 2021.

where n_{elem} refers to the number of elements of the meshed model, and σ_i and V_i represents the stress and volume, respectively, of the considered element. The computed homogenised stress is the "true" measure of the stress.

The results of cylinder compression in figure 8 are highly concurrent to the single element test in compression. The non-conformity to the experimental results at large strain in non-associated plasticity persists. Convergent results for the mesh geometries of different element size ℓ_{elem} affirms mesh independence of the proposed constitutive mathematical model. The equivalent plastic strain contour in figure 9 for a uniformly compressing cylindrical geometry shows even plastic deformation throughout the meshed body for all ℓ_{elem}.

In a way to verify the robustness of the proposed constitutive model, the time incrementation graph plotted in figure 10a proves helpful. The time increment dt remains relatively consistent to the specified maximum time increment $dt_{max} = 0.0133\,\text{s}$ through the course of simulation as observed from the flat graph for the meshes irrespective of ℓ_{elem} under significant strain of 40 %. The continuity of the incrementation process exhibited by the proposed non-iterative scheme is solid testimony to its robustness. Evenly-spaced yielding data provided as input also acts as a factor for the solver to process the simulations smoothly.

The figure 10b illustrates the time required due to computational effort on the solver. Computational costs increase with an increase in the number of elements owing to mesh refinement. Nevertheless, both plastic flow rules yield convergent results with relative ease, attributable to the non-iterative computation process.

4.4. Dog-bone tension test

In another attempt to establish the functionality of the proposed non-iterative scheme for a realistic geometry, a dog-bone specimen, as shown in figure 11 is numerically simulated for tension test. The specimen has an overall length $L_x = 100\,\text{mm}$, width of the narrow portion $L_y = 40\,\text{mm}$ and thickness $L_z = 4\,\text{mm}$. The effective length (gauge length) at the dog-bone's central narrow portion is $D_x = 40\,\text{mm}$ which gradually broadens at either ends of the gauge length into the gripping section radially has the curvature radius $R_c = 30\,\text{mm}$.

Applying symmetrical dissections along xy and xz-planes generate a one-fourth model of the dog-bone specimen depicted in solid outlines on the left

Please cite this article as:
V. Laheri, P. Hao, F.A. Gilabert.
"Efficient non-iterative modelling of pressure-dependent plasticity using paraboloidal yield criterion".
International Journal of Mechanical Sciences (2021), DOI: https://doi.org/10.1016/j.ijmecsci.2021.106988
Received: 18 Jul 2021, Revised: 25 Oct 2021, Accepted: 5 Dec 2021.

of the assembly 11. The resultant symmetrical part geometry of the model is illustrated with boundary and load conditions in the centre of the assembly figure. An instance of the mesh generated for element size $\ell_{elem} = 1\,\text{mm}$ is shown on the right side of the figure. A constant smaller mesh size $\ell_{elem} = 0.5\,\text{mm}$ is maintained through the thickness, causing to increase in the number of elements that ensures a correct resolution of stresses and strains.

The specimen is tested under tension for strain $\varepsilon = 23\,\%$ which is comparatively large than the epoxy polymer can withstand, since epoxy resins typically fail sooner [26]. However, no fracture model is deliberately assumed so as to concentrate on evaluating the mathematical implementations for constitutive elastoplastic models under large strains.

Figure 12a shows the homogenised (see equations (60) and (61)) true stress-strain curve, whereas figure 12b depicts the graph of homogenised true stress plotted against the engineering strain. The engineering strain is computed as the ratio of the applied displacement at RP to the specimen length. The curves in figure 12 are accurately convergent for both the flow rules, irrespective of element size ℓ_{elem}.

The maximum principal stress contour on the specimen after complete loading is consistently similar for both the flow rules plotted in the figure 13 with a homogeneous distribution of stress across the gauge section. The concurrence of the two flow rules is also verifiable by lateral contraction in uniaxial displacement contour plot 14 (top), where U_{zz} is obtained along by the thickness in xz-plane of the specimen. Since both plastic flow rules yield similar results, the associated flow rule can effectively replace the non-associated flow rule. The substitution will reduce the labours of extracting an additional parameter ν^p through elaborate experimental set-ups.

As shown in the figure 15a, the plot for time increment dt through simulation time t exhibits an asymptotic continuity at the limiting value of $dt = 0.0023\text{s}$ for all flow rules and mesh sizes. It adds to prove the higher convergence of computational approach and the inherent robustness of the proposed algorithm that discourages iterative computation of plasticity measures throughout the simulation process. Figure 15b demonstrates increased computational effort with

Please cite this article as:
V. Laheri, P. Hao, F.A. Gilabert.
"Efficient non-iterative modelling of pressure-dependent plasticity using paraboloidal yield criterion".
International Journal of Mechanical Sciences (2021), DOI: https://doi.org/10.1016/j.ijmecsci.2021.106988
Received: 18 Jul 2021, Revised: 25 Oct 2021, Accepted: 5 Dec 2021.

increased mesh refinement and the relative adeptness of mathematical implementation for non-associated plasticity for yielding convergent results than associated plasticity.

A comparison of the iterative and non-iterative numerical implementations of the mathematical models postulated in [32] and that proposed in this paper, respectively is also conducted. For an in-depth analysis, the dog-bone specimen with $\ell_{elem} = 0.5\,\text{mm}$ producing a finer mesh is simulated for tension test under small strain $\varepsilon = 2.5\,‰$.

Table 5: CPU time for dog-bone tension test simulations

Load	**CPU time** [s]	
	Ref. [32]	Proposed
Tension	7648.60	119.10

The homogenised true stress-strain plot in figure 16a and the maximum principal stress contour plot at the end of simulation in figure 17 obtained using the two mathematical models are coincidental to a great extent. However, the model based on iterative scheme is computationally expensive as can be noted from the table 5, the CPU time it takes to complete the simulation is almost 17 times greater than non-iterative algorithm. The time incrementation plot (refer figure 16b) over the course of simulation also depicts that the iterative scheme requires lower than the prescribed maximum time increment, dt_{max} thereby, increasing the number of incrementation steps to achieve convergence. The non-iterative scheme on the other hand, reaches convergence while maintaining an asymptotic dt_{max} thorugh t.

5. Concluding remarks

An extensive literature survey establishes that the paraboloidal yield criterion is an excellent plasticity measure for the pressure dependent but rate and temperature-independent polymer description. The paper introduces an elasto-plastic constitutive model using continuum approach employing this yield criterion with mathematical derivation for both associated and non-associated flow

Please cite this article as:
V. Laheri, P. Hao, F.A. Gilabert.
"Efficient non-iterative modelling of pressure-dependent plasticity using paraboloidal yield criterion".
International Journal of Mechanical Sciences (2021), DOI: https://doi.org/10.1016/j.ijmecsci.2021.106988
Received: 18 Jul 2021, Revised: 25 Oct 2021, Accepted: 5 Dec 2021.

rules. A novel numerical implementation of the non-iterative stress integration scheme is proposed and investigated in this paper. The constitutive relationship utilising the consistent elastoplastic tangent moduli derived for both flow rules importantly captures the pressure-dependent and shear non-linearity characteristics of epoxy matrix while ensuring convergence.

An exact computation of plastic strain is achieved by solving the derived quadratic function and parsing the roots to fulfil the classical consistency conditions. This analytical deduction of plasticity in comparison to the conventional implementation is devoid of numerical scheme using iterative methods. The floating-point operations (FLOPS) for the iterative algorithm becomes uncertain and computationally expensive for no definite knowledge of the iterations to obtain converged results. By eliminating the approximation loops from the subroutine, the proposed model improves computational performance and accuracy significantly.

The numerical simulations using proposed mathematical model for both the flow rules were performed on single-element and two coupon-sized models: cylinder and dog-bone geometries under various load conditions for generic epoxy polymer. An extrapolation method for the evolution of yield stress with plastic strain in the hyper-elastoplastic regime under compression was conceived for linearly piecewise isotropic hardening. The results validated with experiment confirm the functionality of the proposed model under finite strain conditions and are a concrete testimony of its robustness. The difference in computational time of the proposed non-iterative scheme is sparingly shorter than the iterative scheme for the SE analyses. However, this time difference amplifies for the real-sized dog-bone model while the simulation process made several attempts to attain global convergence for the approximated solution.

The compression tests for the associated plasticity yielded a high degree of conformance to the experimental data than the non-associated plasticity model which was initially conformal but diverged under hyper-elastoplastic conditions. Simulation results of the tension test on the dog-bone specimen demonstrated remarkably coincidental results for both the flow rules with uniform stress field along the gauge length.

Please cite this article as:
V. Laheri, P. Hao, F.A. Gilabert.
"Efficient non-iterative modelling of pressure-dependent plasticity using paraboloidal yield criterion".
International Journal of Mechanical Sciences (2021), DOI: https://doi.org/10.1016/j.ijmecsci.2021.106988
Received: 18 Jul 2021, Revised: 25 Oct 2021, Accepted: 5 Dec 2021.

Comparing the results of the proposed and conventional computational implementations showed that both the models can be interchangeably used for non-associated plasticity analysis. However, it is established that the proposed non-iterative model is computationally frugal and speedier with unprecedented accuracy. Although the epoxy materials at macroscale are observed to fail at a low strain range, this implementation will undoubtedly uphold the computational mechanism unto failure with improved computational efficiency. It becomes requisite at microscale level where much larger strains are expected [26].

The study of the proposed implementation for pressure-dependent elasto-plastic model coupled with the damage processes can ideally define mechanical response of the polymer material. It can be effectively used for multiscale and micromechanical analyses of composite materials where different local stress states are expected.

6. Appendices

CRediT author statement

V. Laheri: Conceptualization, investigation, methodology, software, visualisation, validation, writing - original draft, data curation, formal analysis. **P. Hao**: Software, validation, writing - review and editing. **F. A. Gilabert**: Conceptualization, methodology, software, resources, formal analysis, writing - review & editing, supervision, funding acquisition.

Acknowledgments

Financial support from "Bijzonder Onderzoeksfonds" (BOF.STG.2018.0030.01) by Ghent University is gratefully acknowledged. The authors would also like to thank the funding by the ICON project ProPeL, which fits in the MacroModelMat (M3) research program, coordinated by Siemens (Siemens Digital Industries Software, Belgium), and also by SIM (Strategic Initiative Materials in Flanders) and VLAIO (Flemish government agency Flanders Innovation & Entrepreneurship). The authors extend their sincerest gratitude towards the reviewers' insight-

Please cite this article as:
V. Laheri, P. Hao, F.A. Gilabert.
"Efficient non-iterative modelling of pressure-dependent plasticity using paraboloidal yield criterion".
International Journal of Mechanical Sciences (2021), DOI: https://doi.org/10.1016/j.ijmecsci.2021.106988
Received: 18 Jul 2021, Revised: 25 Oct 2021, Accepted: 5 Dec 2021.

ful comments, suggestions and recommendations that were highly influential in improving the quality of this paper.

References

[1] E. M. Arruda and M. C. Boyce. Evolution of plastic anisotropy in amorphous polymers during finite straining. *International Journal of Plasticity*, 9:697–720, 1993.

[2] A. Arteiro, G. Catalanotti, A. R. Melro, P. Linde, and P. P. Camanho. Micro-mechanical analysis of the in situ effect in polymer composite laminates. *Composite Structures*, 116: 827–840, 2014. ISSN 02638223. doi:10.1016/j.compstruct.2014.06.014.

[3] A. Arteiro, G. Catalanotti, A. R. Melro, P. Linde, and P. P. Camanho. Micro-mechanical analysis of the effect of ply thickness on the transverse compressive strength of polymer composites. *Composites Part A: Applied Science and Manufacturing*, 79:127–137, 2015. ISSN 1359835X. doi:10.1016/j.compositesa.2015.09.015.

[4] E. Ballatore. The damage crack model. In Alberto Carpinteri, editor, *Nonlinear Crack Models for NonmetallicMaterials*, pages 27–76. Springer Netherlands, Dordrecht, 1999. ISBN 978-94-011-4700-2. doi:10.1007/978-94-011-4700-2_2.

[5] P. A. Du Bois, S. Kolling, M. Koesters, and T. Frank. Material behaviour of polymers under impact loading. *International Journal of Impact Engineering*, 32(5):725–740, 2006. ISSN 0734743X. doi:10.1016/j.ijimpeng.2005.02.007.

[6] P. B. Bowden and J. A. Jukes. The plastic flow of isotropic polymers. *Journal of Materials Science*, 7:52–63, 1972. doi:10.1007/BF00549550.

[7] M. C. Boyce, D. M. Parks, and A. S. Argon. Large inelastic deformation of glassy polymers. part I: rate dependent constitutive model. *Mechanics of Materials*, 7(1):15–33, 1988. ISSN 01676636. doi:10.1016/0167-6636(88)90003-8.

[8] R. M. Caddell, R. S. Raghava, and A. G. Atkins. Pressure dependent yield criteria for polymers. *Materials Science and Engineering*, 13(2):113–120, 1974. ISSN 00255416. doi:10.1016/0025-5416(74)90179-7.

[9] L. P. Canal, J. Segurado, and J. LLorca. Failure surface of epoxy-modified fiber-reinforced composites under transverse tension and out-of-plane shear. *International Journal of Solids and Structures*, 46(11):2265–2274, 2009. ISSN 0020-7683. doi:10.1016/j.ijsolstr.2009.01.014.

[10] Giro Candelario, Alicia Cordero, Juan R. Torregrosa, and María P. Vassileva. An optimal and low computational cost fractional Newton-type method for solving nonlinear equations. *Applied Mathematics Letters*, 124:107650, February 2022. ISSN 0893-9659. doi:10.1016/j.aml.2021.107650. URL https://www.sciencedirect.com/science/article/pii/S0893965921003487.

[11] M. N. Charalambides and G. D. Dean. Constitutive models and their data requirements for

Please cite this article as:
V. Laheri, P. Hao, F.A. Gilabert.
"Efficient non-iterative modelling of pressure-dependent plasticity using paraboloidal yield criterion".
International Journal of Mechanical Sciences (2021), DOI: https://doi.org/10.1016/j.ijmecsci.2021.106988
Received: 18 Jul 2021, Revised: 25 Oct 2021, Accepted: 5 Dec 2021.

use in finite element analysis of adhesives underimpact loading. *Project PAJ2 Dynamic Performance of Adhesively Bonded Joints*, CMMT(A)59, 1997.

[12] B. D. Coleman and W. Noll. The thermodynamics of elastic materials with heat conduction and viscosity. *The Foundations of Mechanics and Thermodynamics*, page 2, 1963.

[13] C. A. Coulomb. Essai sur une application des regles des maximis et minimis a quelquels problemesde statique relatifs, a la architecture. *Mem. Acad. Roy. Div. Sav*, Vol. 7:343–387., 1776.

[14] R. R. de Sousa Junior, J. R. Gouveia, N. M. Ito, and D. J. dos Santos. Failure prediction of hybrid composite using Arcan's device and Drucker-Prager model. *Polymer Testing*, 58: 256–261, April 2017. ISSN 0142-9418. doi:10.1016/j.polymertesting.2017.01.001. URL https://www.sciencedirect.com/science/article/pii/S0142941816313046.

[15] Gustavo H. B. Donato and M. Bianchi. Numerical modeling of uneven thermoplastic polymers behaviour using experimental stress-strain data and pressure dependent von Mises yield criteria to improve design practices. *11th International Conference on the Mechanical Behavior of Materials (ICM11)*, 10:1871–1876, 2011. ISSN 1877-7058. doi:10.1016/j.proeng.2011.04.311.

[16] D. C. Drucker and W. Prager. Soil mechanics and plastic analysis or limit design. *Quarterly of Applied Mathematics*, 10(2):157–165, 1952. ISSN 0033-569X, 1552-4485. doi:10.1090/qam/48291.

[17] B. C. Duncan, G. D. Dean, and B. E. Read. Prediction of the performance of adhesives under impact loading. *Project PAJ2 Dynamic Performance of Adhesively Bonded Joints*, CMMT(B)162:7, 1998.

[18] B. Fiedler, M. Hojo, S. Ochiai, K. Schulte, and M. Ando. Failure behavior of an epoxy matrix under different kinds of static loading. *Composites Science and Technology*, 61(11): 1615–1624, 2001. ISSN 02663538. doi:10.1016/S0266-3538(01)00057-4.

[19] B. Fiedler, M. Hojo, S. Ochiai, K. Schulte, and M. Ochi. Finite-element modeling of initial matrix failure in CFRP under static transverse tensile load. *Composites Science and Technology*, 61(1):95–105, 2001. ISSN 02663538. doi:10.1016/S0266-3538(00)00198-6.

[20] H. Ghayoor, C. C. Marsden, S. V. Hoa, and A. R. Melro. Numerical analysis of resin-rich areas and their effects on failure initiation of composites. *Composites Part A: Applied Science and Manufacturing*, 117:125–133, 2019. ISSN 1359835X. doi:10.1016/j.compositesa.2018.11.016.

[21] E. Ghorbel. A viscoplastic constitutive model for polymeric materials. *International Journal of Plasticity*, 24(11):2032–2058, 2008. ISSN 07496419. doi:10.1016/j.ijplas.2008.01.003.

[22] C. González and J. LLorca. Mechanical behavior of unidirectional fiber-reinforced polymers under transverse compression: Microscopic mechanisms and modeling. *Composites Science and Technology*, 67(13):2795–2806, 2007. ISSN 0266-3538.

[23] F. J. Guild, K. D. Potter, J. Heinrich, R. D. Adams, and M. R. Winsom. Understanding and control of adhesive crack propagation in bonded joints between carbon fibre composite

Please cite this article as:
V. Laheri, P. Hao, F.A. Gilabert.
"Efficient non-iterative modelling of pressure-dependent plasticity using paraboloidal yield criterion".
International Journal of Mechanical Sciences (2021), DOI: https://doi.org/10.1016/j.ijmecsci.2021.106988
Received: 18 Jul 2021, Revised: 25 Oct 2021, Accepted: 5 Dec 2021.

adherends II. finite element analysis. *International Journal of Adhesion and Adhesives*, 21 (6):445–453, 2001. ISSN 01437496. doi:10.1016/S0143-7496(01)00021-5.

[24] H. Hara and K. Shizawa. Homogenized molecular chain plasticity simulation for crystalline polymer using craze evolution model based on chemical kinetics. *International Journal of Mechanical Sciences*, 101-102:180–195, 2015. ISSN 0020-7403. doi:10.1016/j.ijmecsci.2015.07.022.

[25] C. He, J. Ge, D. Qi, J. Gao, Y. Chen, J. Liang, and D. Fang. A multiscale elasto-plastic damage model for the nonlinear behavior of 3D braided composites. *Composites Science and Technology*, 171:21–33, 2019. ISSN 0266-3538. doi:10.1016/j.compscitech.2018.12.003.

[26] T. Hobbiebrunken, B. Fiedler, M. Hojo, and M. Tanaka. Experimental determination of the true epoxy resin strengthusing micro-scaled specimens. *Composites: Part A*, 38:814818, 2007. doi:10.1016/j.compositesa.2006.08.006.

[27] J. Johnsen, A. H. Clausen, F. Grytten, A. Benallal, and O. S. Hopperstad. A thermo-elasto-viscoplastic constitutive model for polymers. *Journal of the Mechanics and Physics of Solids*, 124:681–701, 2019. ISSN 00225096. doi:10.1016/j.jmps.2018.11.018.

[28] A. J. Kinloch. *Fracture behaviour of polymers*. Springer Science & Business Media, 2013.

[29] S. Kolling, A. Haufe, and M. Feucht. SAMP: A semi-analytical model for the simulation of polymers. In *DYNAmore GmbH*, pages 27–52, 2005.

[30] A. Krairi and I. Doghri. A thermodynamically-based constitutive model for thermoplastic polymers coupling viscoelasticity, viscoplasticity and ductile damage. *International Journal of Plasticity*, 60:163–181, 2014. ISSN 07496419. doi:10.1016/j.ijplas.2014.04.010.

[31] W. N. Mascarenhas, C. H. Ahrens, and A. Ogliari. Design criteria and safety factors for plastic components design. *Materials and Design*, page 5, 2004. doi:10.1016/j.matdes.2003.10.003.

[32] A. R. Melro. *Analytical and numerical modelling of damage and fracture of advanced composites*. Doctoral Thesis, University of Porto, Porto, Portugal, 2011.

[33] A. R. Melro, P. P. Camanho, F. M. Andrade Pires, and S. T. Pinho. Numerical simulation of the non-linear deformation of 5-harness satin weaves. *Computational Materials Science*, 61:116–126, 2012. ISSN 09270256. doi:10.1016/j.commatsci.2012.04.010.

[34] A. R. Melro, P. P. Camanho, F. M. Andrade Pires, and S. T. Pinho. Micromechanical analysis of polymer composites reinforced by unidirectional fibres: Part I constitutive modelling. *International Journal of Solids and Structures*, 50(11):1897–1905, 2013. ISSN 00207683. doi:10.1016/j.ijsolstr.2013.02.009.

[35] A. R. Melro, P. P. Camanho, F. M. Andrade Pires, and S. T. Pinho. Micromechanical analysis of polymer composites reinforced by unidirectional fibres: Part II micromechanical analyses. *International Journal of Solids and Structures*, 50(11):1906–1915, 2013. ISSN 00207683. doi:10.1016/j.ijsolstr.2013.02.007.

[36] L. Ongchin and S. S. Sternstein. Yield criteria for plastic deformation on glassy high polymers in general stress fields. *ACS Polymer Prep.*, 10:1117, 1969.

Please cite this article as:
V. Laheri, P. Hao, F.A. Gilabert.
"Efficient non-iterative modelling of pressure-dependent plasticity using paraboloidal yield criterion".
International Journal of Mechanical Sciences (2021), DOI: https://doi.org/10.1016/j.ijmecsci.2021.106988
Received: 18 Jul 2021, Revised: 25 Oct 2021, Accepted: 5 Dec 2021.

[37] H. Park, S. Yang, J. Han, and M. Cho. Prediction of quasistatic constitutive equations of moisture-absorbed epoxy polymers using atomistic simulations. *Extreme Mechanics Letters*, 41:100983, 2020. ISSN 2352-4316. doi:10.1016/j.eml.2020.100983.

[38] K. G. W. Pijnenburg, Th. Seelig, and E. van der Giessen. Successively refined models for crack tip plasticity in polymer blends. *European Journal of Mechanics - A/Solids*, 24(5): 740–756, 2005. ISSN 0997-7538. doi:10.1016/j.euromechsol.2005.04.005.

[39] X. Poulain, A. A. Benzerga, and R. K. Goldberg. Finite-strain elasto-viscoplastic behavior of an epoxy resin: Experiments and modeling in the glassy regime. *International Journal of Plasticity*, 62:138–161, 2014. ISSN 07496419. doi:10.1016/j.ijplas.2014.07.002.

[40] D. Pulungan, G. Lubineau, A. Yudhanto, R. Yaldiz, and W. Schijve. Identifying design parameters controlling damage behaviors of continuous fiber-reinforced thermoplastic composites using micromechanics as a virtual testing tool. *International Journal of Solids and Structures*, 117:177–190, 2017. ISSN 00207683. doi:10.1016/j.ijsolstr.2017.03.026.

[41] R. Raghava, R. M. Caddell, and G. S. Y. Yeh. The macroscopic yield behaviour of polymers. *Journal of Materials Science*, 8(2):225–232, 1973. ISSN 0022-2461, 1573-4803. doi:10.1007/BF00550671.

[42] R. S. Raghava and R. M. Caddell. A macroscopic yield criterion for crystalline polymers. *International Journal of Mechanical Sciences*, 15(12):967–974, 1973. ISSN 00207403. doi:10.1016/0020-7403(73)90106-9.

[43] W. Retting. *Mechanik der Kunststoffe: die mechanischen eigenschaften von polymerwerkstoffen*, volume 125 p.; Ill., graph. Darst. München: Wien: Hanser, 1992. ISBN 3446161015; 9783446161016.

[44] Th. Seelig and E. Van der Giessen. A cell model study of crazing and matrix plasticity in rubber-toughened glassy polymers. *Proceedings of the 17th International Workshop on Computational Mechanics of Materials*, 45(3):725–728, 2009. ISSN 0927-0256. doi:10.1016/j.commatsci.2008.05.024.

[45] R. Seltzer, A. P. Cisilino, P. M. Frontini, and Yiu-W. Mai. Determination of the DruckerPrager parameters of polymers exhibiting pressure-sensitive plastic behaviour by depth-sensing indentation. *International Journal of Mechanical Sciences*, 53(6):471–478, 2011. ISSN 0020-7403. doi:10.1016/j.ijmecsci.2011.04.002.

[46] R. Sepasdar and M. Shakiba. Overcoming the convergence difficulty of cohesive zone models through a Newton-Raphson modification technique. *Engineering Fracture Mechanics*, 233:107046, June 2020. ISSN 0013-7944. doi:10.1016/j.engfracmech.2020.107046. URL https://www.sciencedirect.com/science/article/pii/S0013794419314249.

[47] H. Singh, M. Gupta, and P. Mahajan. Reduced order multiscale modeling of fiber reinforced polymer composites including plasticity and damage. *Mechanics of Materials*, 111:35–56, 2017. ISSN 0167-6636. doi:10.1016/j.mechmat.2017.05.003.

[48] G. SPATHIS. Theory for the plastic deformation of glassy polymers. *Journal of Materials Science*, 32(7):1943–1950, 1997. ISSN 1573-4803. doi:10.1023/A:1018533613296. URL

Please cite this article as:
V. Laheri, P. Hao, F.A. Gilabert.
"Efficient non-iterative modelling of pressure-dependent plasticity using paraboloidal yield criterion".
International Journal of Mechanical Sciences (2021), DOI: https://doi.org/10.1016/j.ijmecsci.2021.106988
Received: 18 Jul 2021, Revised: 25 Oct 2021, Accepted: 5 Dec 2021.

https://doi.org/10.1023/A:1018533613296.

[49] S. Stark, S. Roth, P. Neumeister, and H. Balke. Modifications of the Newton-Raphson method for finite element simulations in ferroelectroelasticity. *International Journal of Solids and Structures*, 50(5):773–780, March 2013. ISSN 0020-7683. doi:10.1016/j.ijsolstr.2012.11.008. URL https://www.sciencedirect.com/science/article/pii/S0020768312004714.

[50] R. P. Tavares, A. R. Melro, M. A. Bessa, A. Turon, W. K. Liu, and P. P. Camanho. Mechanics of hybrid polymer composites: analytical and computational study. *Computational Mechanics*, 57(3):405–421, 2016. ISSN 0178-7675, 1432-0924. doi:10.1007/s00466-015-1252-0.

[51] E. Totry, C. González, and J. LLorca. Prediction of the failure locus of C/PEEK composites under transverse compression and longitudinal shear through computational micromechanics. *Composites Science and Technology*, 68(15):3128–3136, 2008. ISSN 0266-3538. doi:10.1016/j.compscitech.2008.07.011.

[52] E. Totry, J. M. Molina-Aldareguía, C. González, and J. LLorca. Effect of fiber, matrix and interface properties on the in-plane shear deformation of carbon-fiber reinforced composites. *Composites Science and Technology*, 70(6):970–980, 2010. ISSN 0266-3538. doi:10.1016/j.compscitech.2010.02.014.

[53] N. W. Tschoegl. Failure surfaces in principal stress space. *Polymer Science Symposium*, 32:239–267, 1971.

[54] L. F. Varandas, A. Arteiro, M. A. Bessa, A. R. Melro, and G. Catalanotti. The effect of through-thickness compressive stress on mode II interlaminar crack propagation: A computational micromechanics approach. *Composite Structures*, 182:326–334, 2017. ISSN 02638223. doi:10.1016/j.compstruct.2017.09.020.

[55] L. F. Varandas, G. Catalanotti, A. R. Melro, and B. G. Falzon. On the importance of nesting considerations for accurate computational damage modelling in 2d woven composite materials. *Computational Materials Science*, 172:109323, 2020. ISSN 09270256. doi:10.1016/j.commatsci.2019.109323.

[56] L. F. Varandas, G. Catalanotti, A. R. Melro, R. P. Tavares, and B. G. Falzon. Micromechanical modelling of the longitudinal compressive and tensile failure of unidirectional composites: The effect of fibre misalignment introduced via a stochastic process. *International Journal of Solids and Structures*, 203:157–176, 2020. ISSN 00207683. doi:10.1016/j.ijsolstr.2020.07.022.

[57] J. C. Volmer, T. W. J. de Geus, and R. H. J. Peerlings. Improving the initial guess for the Newton-Raphson protocol in time-dependent simulations. *Journal of Computational Physics*, 420:109721, November 2020. ISSN 0021-9991. doi:10.1016/j.jcp.2020.109721. URL https://www.sciencedirect.com/science/article/pii/S0021999120304952.

[58] M. R. Wisnom. Size effects in the testing of fibre-composite materials. *Composites Science and Technology*, 59(13):1937–1957, 1999. ISSN 0266-3538.

Please cite this article as:
V. Laheri, P. Hao, F.A. Gilabert.
"Efficient non-iterative modelling of pressure-dependent plasticity using paraboloidal yield criterion".
International Journal of Mechanical Sciences (2021), DOI: https://doi.org/10.1016/j.ijmecsci.2021.106988
Received: 18 Jul 2021, Revised: 25 Oct 2021, Accepted: 5 Dec 2021.

doi:https://doi.org/10.1016/S0266-3538(99)00053-6.

[59] A. S. Wronski and M. Pick. Pyramidal yield criteria for epoxides. *Journal of Materials Science*, 12(1):28–34, January 1977. ISSN 1573-4803. doi:10.1007/BF00738468. URL https://doi.org/10.1007/BF00738468.

[60] P. D. Wu and E. Van Der Giessen. On improved network models for rubber elasticity and their applications to orientation hardening in glassy polymers. *Journal of the Mechanics and Physics of Solids*, 41(3):427–456, 1993. ISSN 00225096. doi:10.1016/0022-5096(93)90043-F.

[61] P. D. Wu and E. Van Der Giessen. Computational aspects of localized deformations in amorphous glassy polymers. *European Journal of Mechanics - A/Solids*, 15(5):799–823, 1996.

Please cite this article as:
V. Laheri, P. Hao, F.A. Gilabert.
"Efficient non-iterative modelling of pressure-dependent plasticity using paraboloidal yield criterion".
International Journal of Mechanical Sciences (2021), DOI: https://doi.org/10.1016/j.ijmecsci.2021.106988
Received: 18 Jul 2021, Revised: 25 Oct 2021, Accepted: 5 Dec 2021.

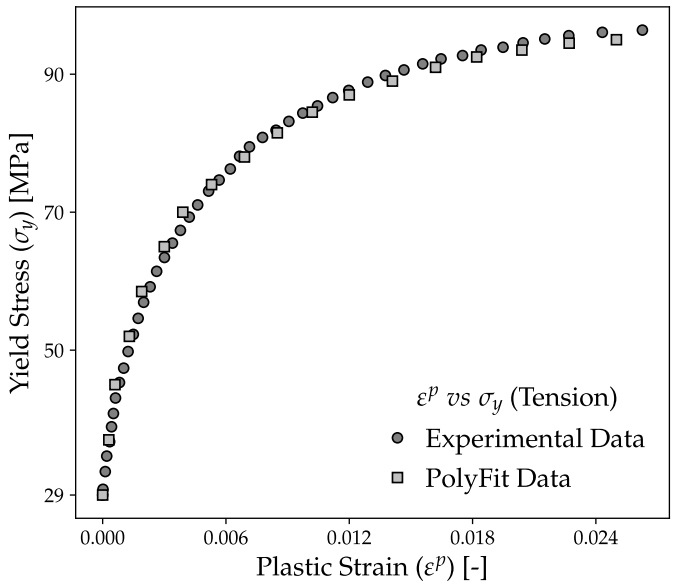

(a) Tension

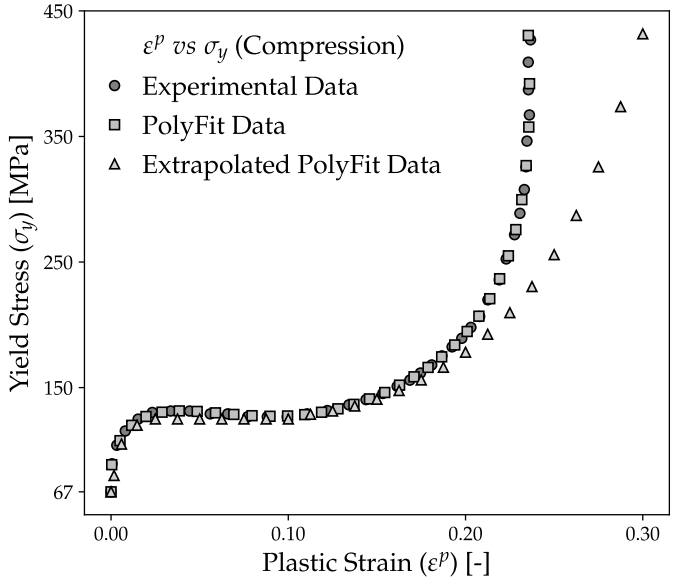

(b) Compression

Figure 1: Evolution of yield stress σ_y concerning plastic strain ϵ^p extracted from the experimental data of Fiedler et al. [18] though polynomial-fitting for tension and compression tests. The $\sigma_y - \epsilon^p$ evolution plot in compression also depicts an additional extrapolated curve.

Please cite this article as:
V. Laheri, P. Hao, F.A. Gilabert.
"Efficient non-iterative modelling of pressure-dependent plasticity using paraboloidal yield criterion".
International Journal of Mechanical Sciences (2021), DOI: https://doi.org/10.1016/j.ijmecsci.2021.106988
Received: 18 Jul 2021, Revised: 25 Oct 2021, Accepted: 5 Dec 2021.

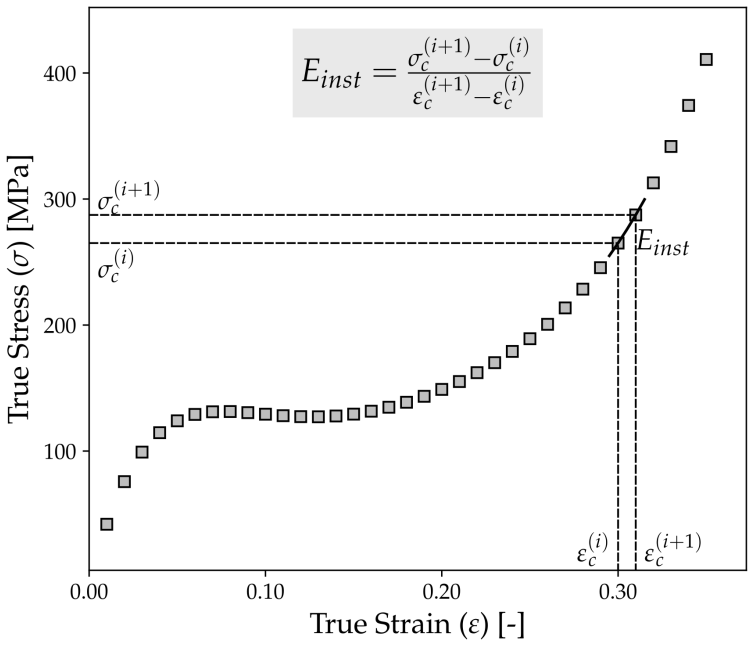

Figure 2: Instantaneous stiffness calculation for extrapolated $\sigma_y - \epsilon^p$ computation in compression.

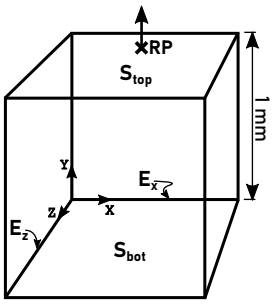

Tension/Compression	Simple Shear
$(+1)U_y^{\mathrm{RP}} + (-1)U_y^{\mathrm{S_{top}}} = 0$	$(+1)U_x^{\mathrm{RP}} + (-1)U_x^{\mathrm{S_{top}}} = 0$
$U_x^{\mathrm{E_x}} = 0$	$U_x^{\mathrm{S_{bot}}} = 0$
$U_y^{\mathrm{S_{bot}}} = 0$	$U_y^{\mathrm{S_{bot}}} = 0$
$U_z^{\mathrm{E_z}} = 0$	$U_y^{\mathrm{S_{top}}} = 0$

Figure 3: Right: A cubic body representing a single element with demarcated surfaces, edges and the reference loading point. Left: Boundary conditions and load of the single element test tabulated for the different loading conditions.

Please cite this article as:
V. Laheri, P. Hao, F.A. Gilabert.
"Efficient non-iterative modelling of pressure-dependent plasticity using paraboloidal yield criterion".
International Journal of Mechanical Sciences (2021), DOI: https://doi.org/10.1016/j.ijmecsci.2021.106988
Received: 18 Jul 2021, Revised: 25 Oct 2021, Accepted: 5 Dec 2021.

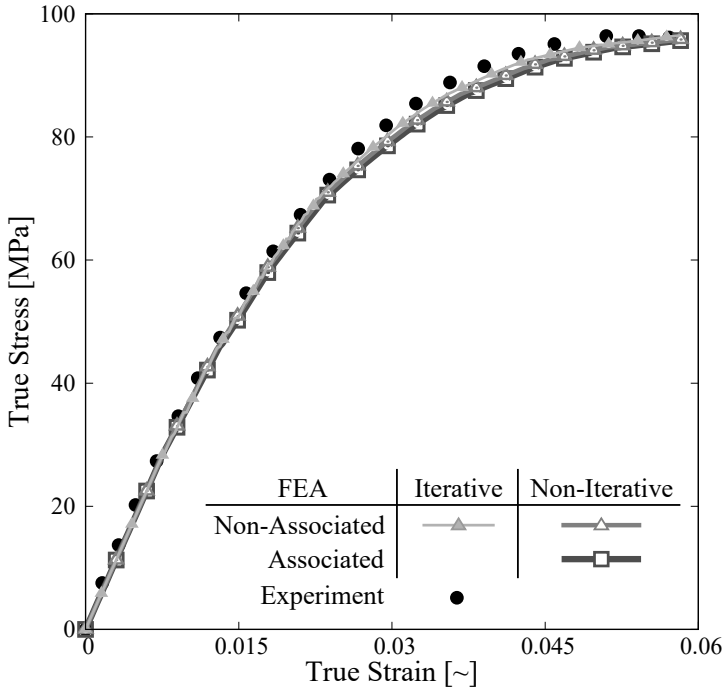

(a) Tension

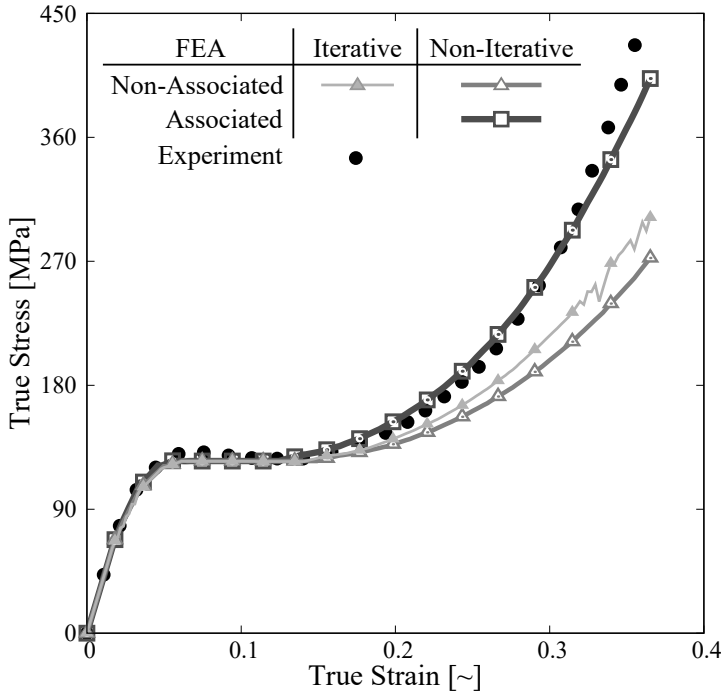

(b) Compression

Please cite this article as:
V. Laheri, P. Hao, F.A. Gilabert.
"Efficient non-iterative modelling of pressure-dependent plasticity using paraboloidal yield criterion".
International Journal of Mechanical Sciences (2021), DOI: https://doi.org/10.1016/j.ijmecsci.2021.106988
Received: 18 Jul 2021, Revised: 25 Oct 2021, Accepted: 5 Dec 2021.

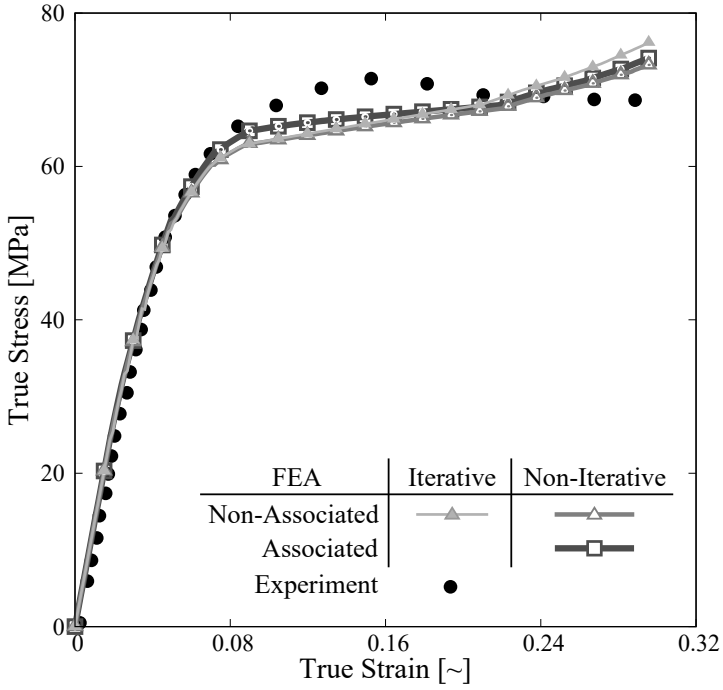

(c) Shear

Figure 4: Stress-strain relationship of single element test for the three loading conditions. The tension curves for both the flow rules are convergent to the experiment, while the compression curve for associated plasticity yields results in agreement to experiment than non-associated plasticity. The deviations from the experimental curve in shear mode is because the yield function is independent of the yielding in shear.

Please cite this article as:
V. Laheri, P. Hao, F.A. Gilabert.
"Efficient non-iterative modelling of pressure-dependent plasticity using paraboloidal yield criterion".
International Journal of Mechanical Sciences (2021), DOI: https://doi.org/10.1016/j.ijmecsci.2021.106988
Received: 18 Jul 2021, Revised: 25 Oct 2021, Accepted: 5 Dec 2021.

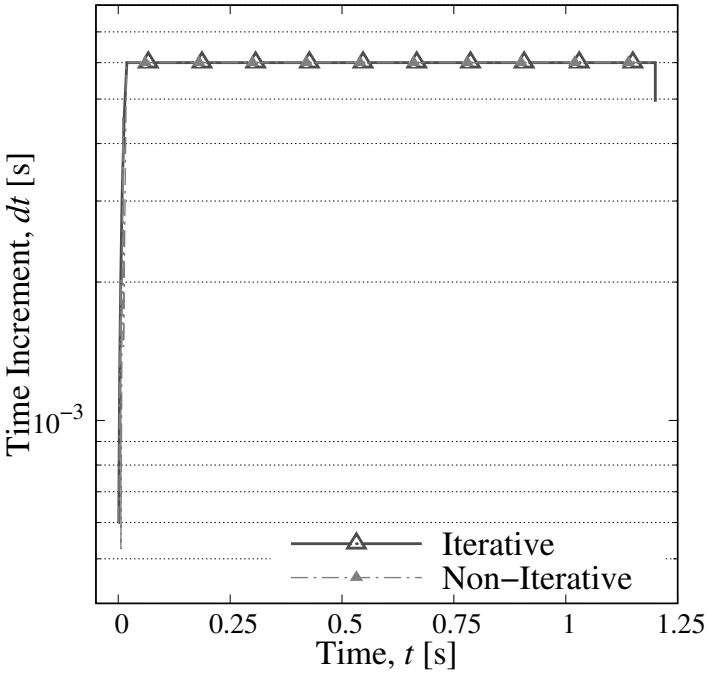

(a) Tension

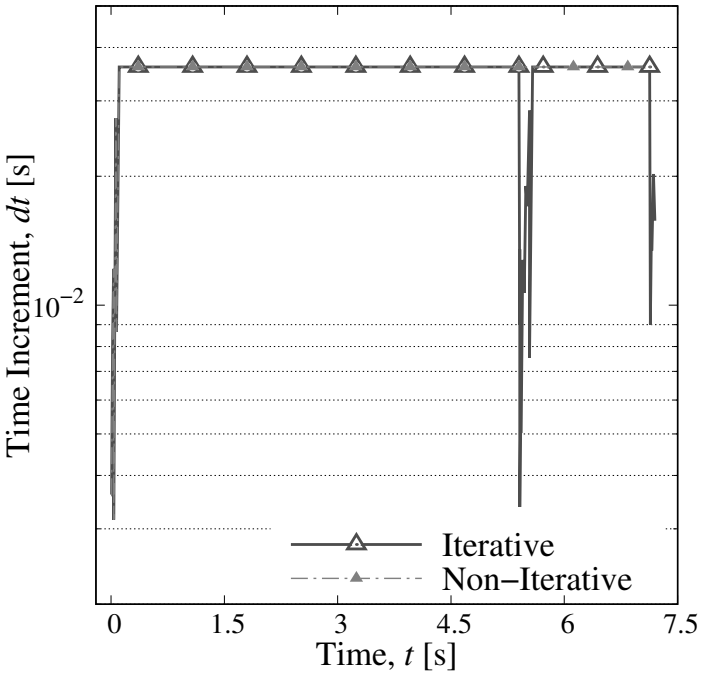

(b) Compression

Please cite this article as:
V. Laheri, P. Hao, F.A. Gilabert.
"Efficient non-iterative modelling of pressure-dependent plasticity using paraboloidal yield criterion".
International Journal of Mechanical Sciences (2021), DOI: https://doi.org/10.1016/j.ijmecsci.2021.106988
Received: 18 Jul 2021, Revised: 25 Oct 2021, Accepted: 5 Dec 2021.

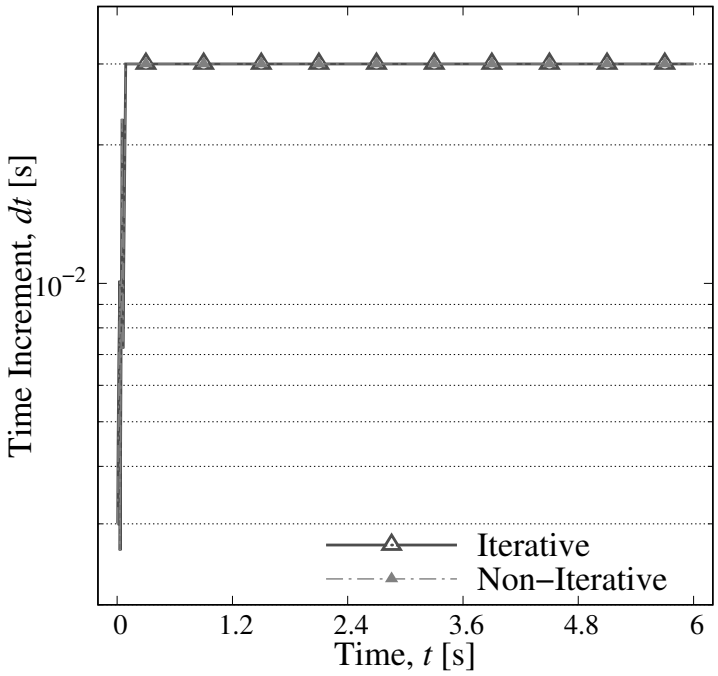

(c) Shear

Figure 5: Time incrementation status of single element test showing even time increment for tension and shear loading modes concerning both mathematical implementations. The compression mode witnesses consistent incrementation with the proposed non-iterative scheme while is crinkly for the iterative numerical scheme.

Please cite this article as:
V. Laheri, P. Hao, F.A. Gilabert.
"Efficient non-iterative modelling of pressure-dependent plasticity using paraboloidal yield criterion".
International Journal of Mechanical Sciences (2021), DOI: https://doi.org/10.1016/j.ijmecsci.2021.106988
Received: 18 Jul 2021, Revised: 25 Oct 2021, Accepted: 5 Dec 2021.

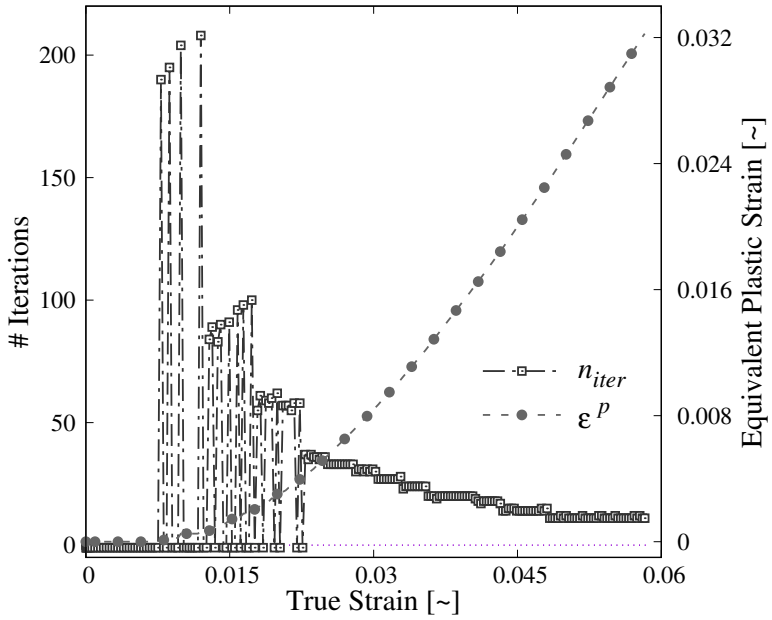

(a) Tension

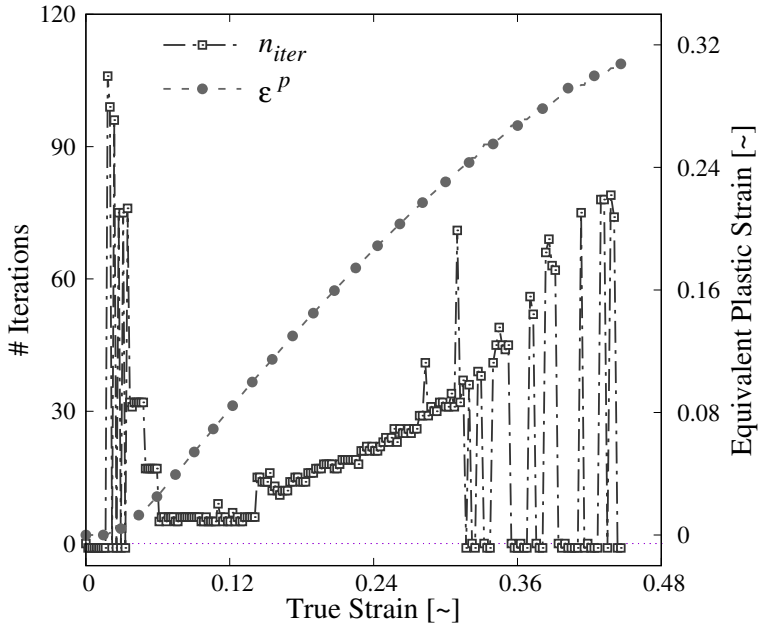

(b) Compression

Please cite this article as:
V. Laheri, P. Hao, F.A. Gilabert.
"Efficient non-iterative modelling of pressure-dependent plasticity using paraboloidal yield criterion".
International Journal of Mechanical Sciences (2021), DOI: https://doi.org/10.1016/j.ijmecsci.2021.106988
Received: 18 Jul 2021, Revised: 25 Oct 2021, Accepted: 5 Dec 2021.

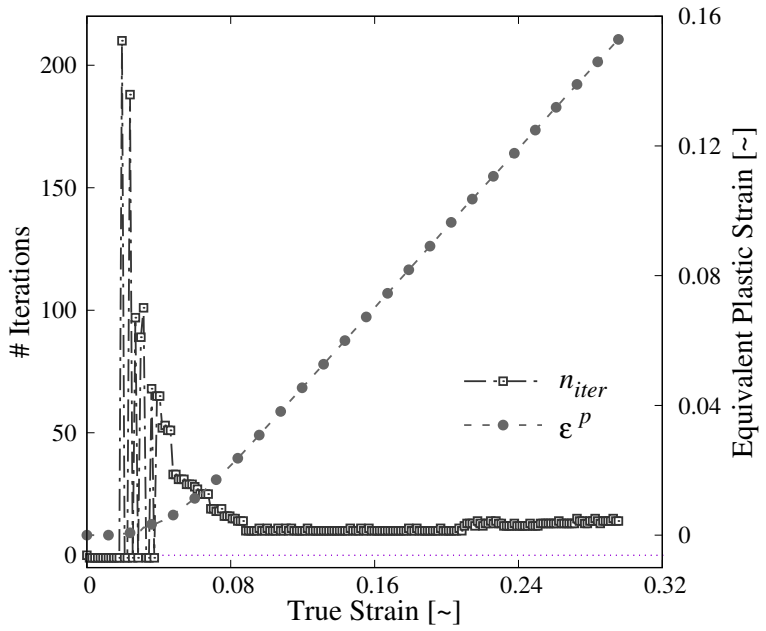

(c) Shear

Figure 6: Iterations counter with respect to the plastic strain evolution using iterative scheme of [32]. The number of iterations is invariable and significantly large for obtaining convergence for the non-linear evolution plastic strain increment. The number of iterations decays as the plastic strain increment attains linearity.

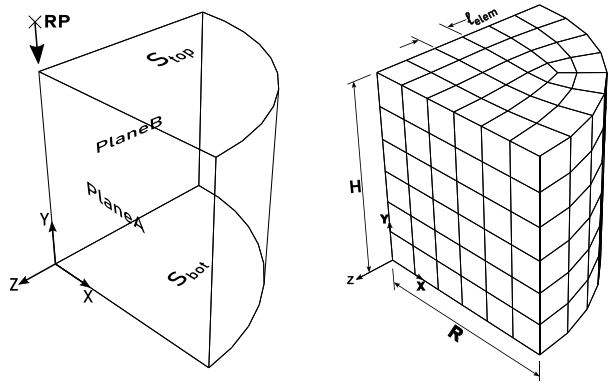

$$(+1)U_y^{\mathrm{RP}} + (-1)U_y^{\mathrm{S_{top}}} = 0$$

$$U_x^{\mathrm{PlaneB}} = 0$$
$$U_y^{\mathrm{S_{bot}}} = 0$$
$$U_z^{\mathrm{PlaneA}} = 0$$

Figure 7: Cylinder compression test specimen and boundary conditions. (Left): Symmetrical model set-up. (Right): Finite element mesh and geometrical dimensions.

Please cite this article as:
V. Laheri, P. Hao, F.A. Gilabert.
"Efficient non-iterative modelling of pressure-dependent plasticity using paraboloidal yield criterion".
International Journal of Mechanical Sciences (2021), DOI: https://doi.org/10.1016/j.ijmecsci.2021.106988
Received: 18 Jul 2021, Revised: 25 Oct 2021, Accepted: 5 Dec 2021.

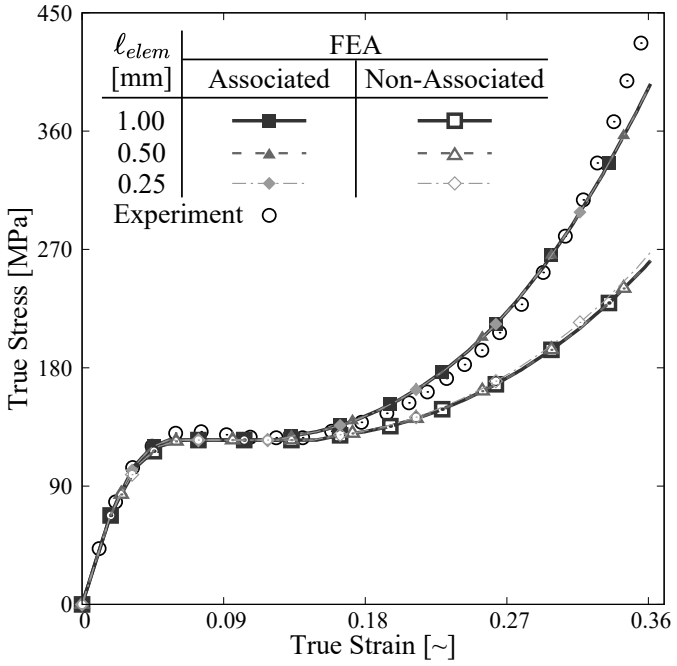

Figure 8: Stress-strain relationship for cylinder compression test resembling the results of single element test and establishing mesh convergence.

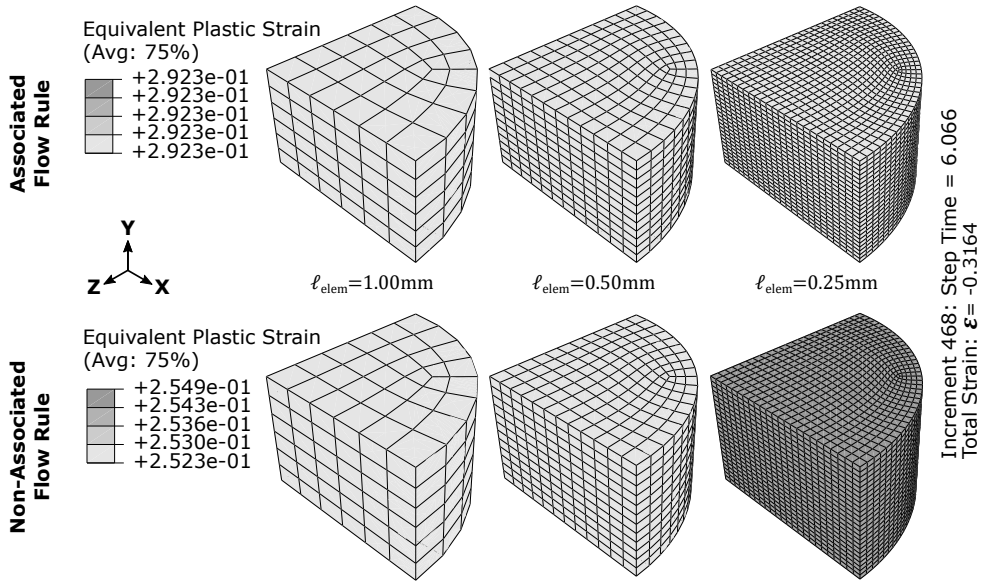

Figure 9: Equivalent plastic strain contour plot for cylinder specimen establishing mesh convergence for the associated and non-associated flow rules.

Please cite this article as:
V. Laheri, P. Hao, F.A. Gilabert.
"Efficient non-iterative modelling of pressure-dependent plasticity using paraboloidal yield criterion".
International Journal of Mechanical Sciences (2021), DOI: https://doi.org/10.1016/j.ijmecsci.2021.106988
Received: 18 Jul 2021, Revised: 25 Oct 2021, Accepted: 5 Dec 2021.

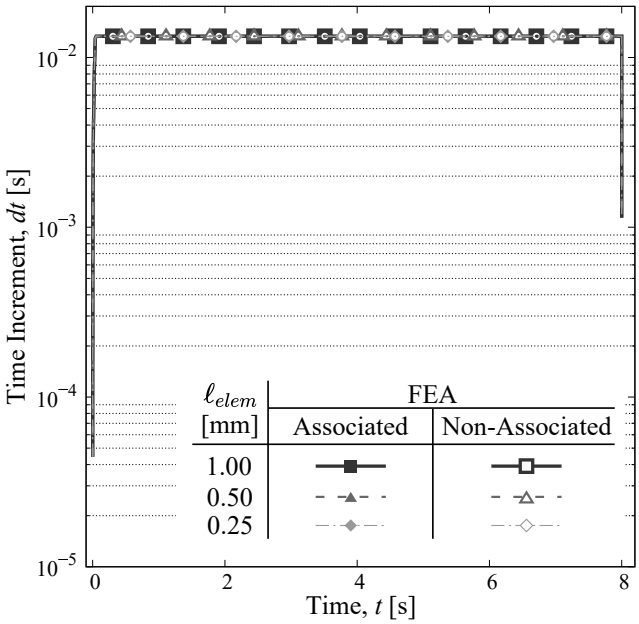

(a) Time incrementation status

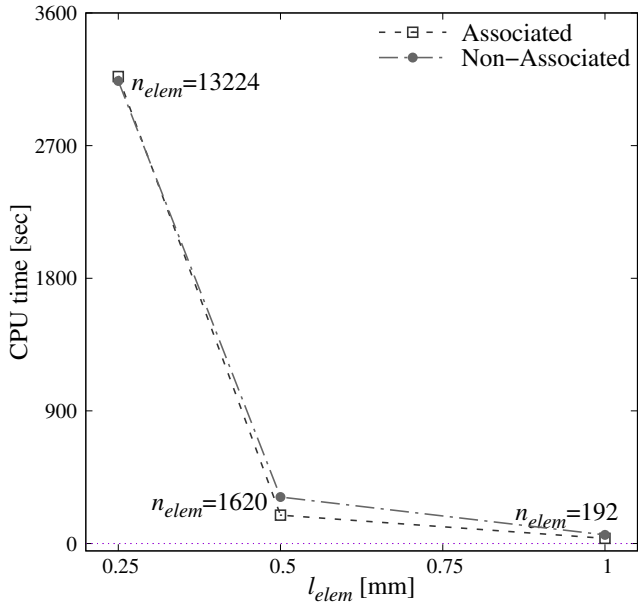

(b) CPU time versus element length

Figure 10: Comparison of the flow rules for the cylinder compression test through time incrementation and computational time consumption of the simulations are shown. Both the flow rules yield convergent results with relative computational ease for different mesh refinements.

Please cite this article as:
V. Laheri, P. Hao, F.A. Gilabert.
"Efficient non-iterative modelling of pressure-dependent plasticity using paraboloidal yield criterion".
International Journal of Mechanical Sciences (2021), DOI: https://doi.org/10.1016/j.ijmecsci.2021.106988
Received: 18 Jul 2021, Revised: 25 Oct 2021, Accepted: 5 Dec 2021.

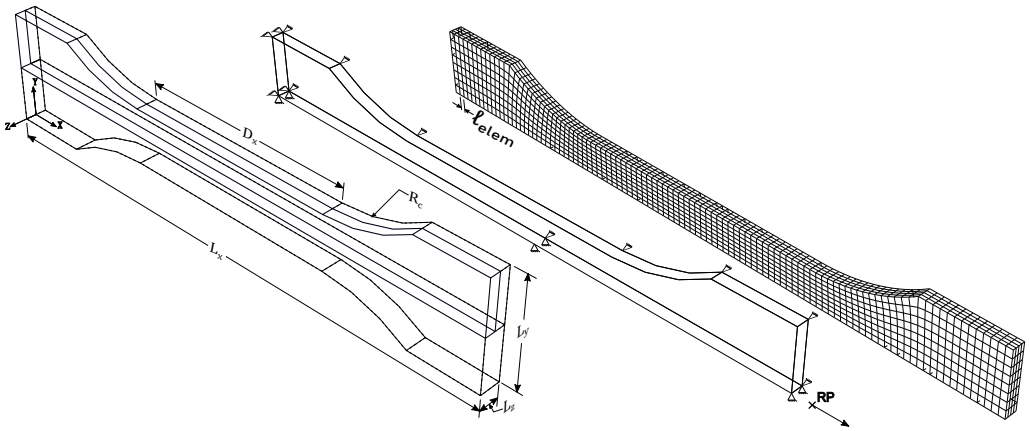

Figure 11: (Left): Geometrical illustration, (Centre): Part geometry with boundary conditions, and (Right): Structured mesh instance of dog-bone tension test specimen.

Please cite this article as:
V. Laheri, P. Hao, F.A. Gilabert.
"Efficient non-iterative modelling of pressure-dependent plasticity using paraboloidal yield criterion".
International Journal of Mechanical Sciences (2021), DOI: https://doi.org/10.1016/j.ijmecsci.2021.106988
Received: 18 Jul 2021, Revised: 25 Oct 2021, Accepted: 5 Dec 2021.

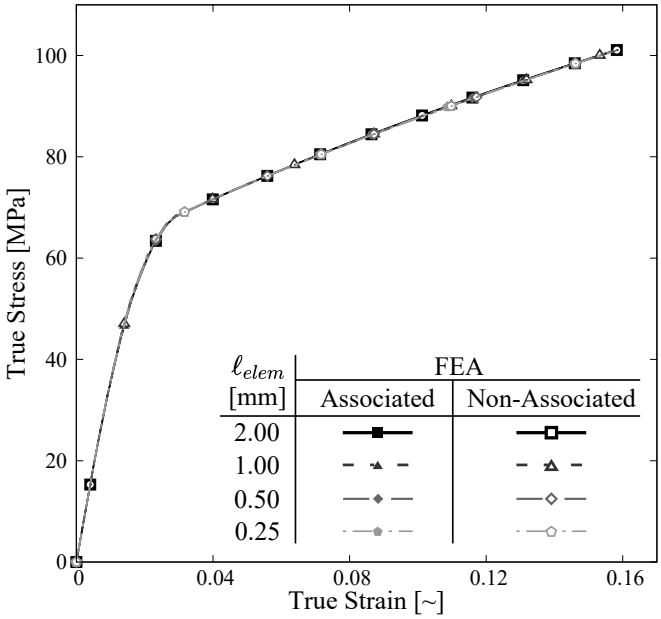

(a) True stress-strain relationship

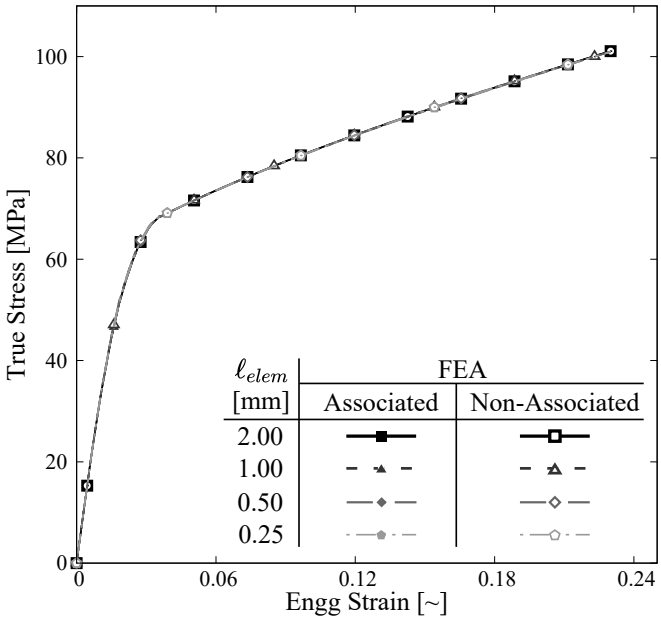

(b) True stress - engineering strain relationship

Figure 12: Stress-strain relationship for the tensile test of dog-bone specimen showing mesh convergence for the associated and non-associated flow rules. The results of both flow rules are also concurrent with each other, therefore ascertaining their interchangeability.

Please cite this article as:
V. Laheri, P. Hao, F.A. Gilabert.
"Efficient non-iterative modelling of pressure-dependent plasticity using paraboloidal yield criterion".
International Journal of Mechanical Sciences (2021), DOI: https://doi.org/10.1016/j.ijmecsci.2021.106988
Received: 18 Jul 2021, Revised: 25 Oct 2021, Accepted: 5 Dec 2021.

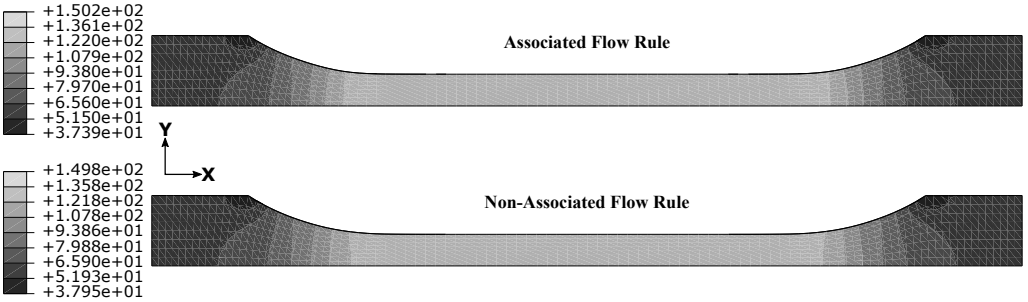

Figure 13: Max principal stress contour plot at the end of tension test on the dog-bone specimen showing similar stress dispersement for the two flow rules. The stress contour is also homogeneous in the gauge section of the specimen.

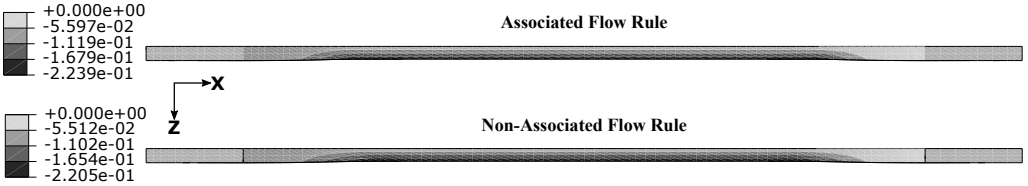

Figure 14: Displacement (U_{zz}) measure in the thickness of dog-bone specimen at the end of tension test showing similar displacement distribution.

Please cite this article as:
V. Laheri, P. Hao, F.A. Gilabert.
"Efficient non-iterative modelling of pressure-dependent plasticity using paraboloidal yield criterion".
International Journal of Mechanical Sciences (2021), DOI: https://doi.org/10.1016/j.ijmecsci.2021.106988
Received: 18 Jul 2021, Revised: 25 Oct 2021, Accepted: 5 Dec 2021.

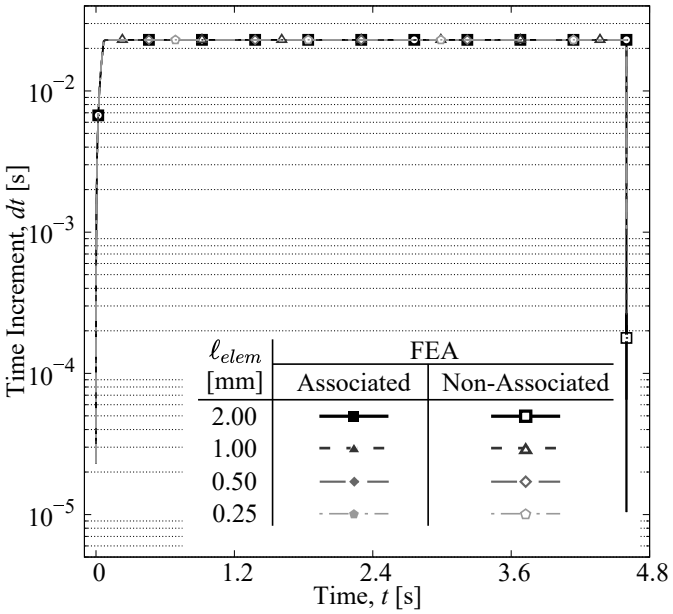

(a) Time incrementation status

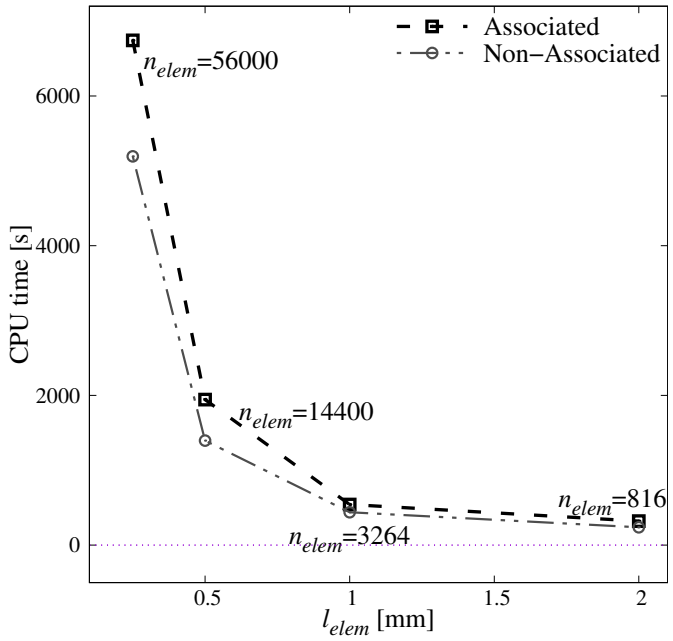

(b) CPU time versus element length

Figure 15: Simulation comparison for the dog-bone tension tests employing the two flow rules show similar computational effort through $dt-t$ graph, while ascertain the speedier convergence of non-associated flow rule through CPU time vs ℓ_{elem} plot.

Please cite this article as:
V. Laheri, P. Hao, F.A. Gilabert.
"Efficient non-iterative modelling of pressure-dependent plasticity using paraboloidal yield criterion".
International Journal of Mechanical Sciences (2021), DOI: https://doi.org/10.1016/j.ijmecsci.2021.106988
Received: 18 Jul 2021, Revised: 25 Oct 2021, Accepted: 5 Dec 2021.

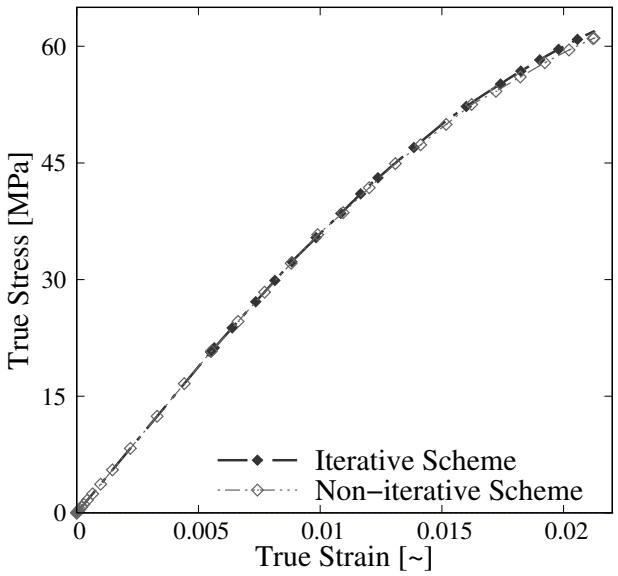

(a) True stress-strain relationship

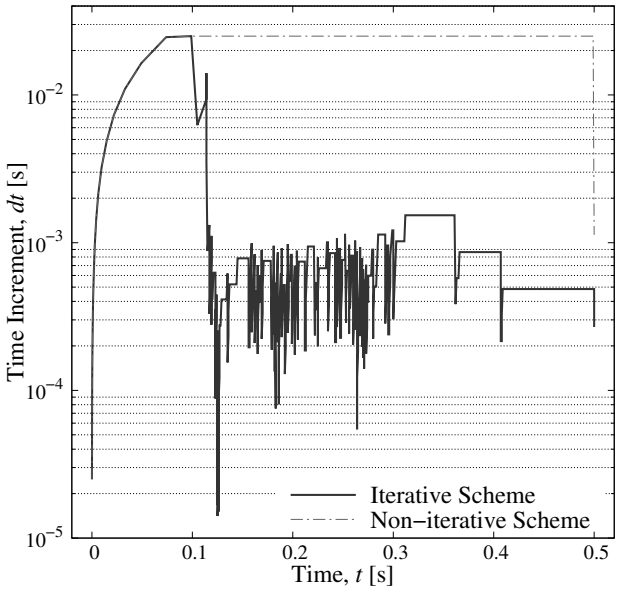

(b) Time incrementation status

Figure 16: Simulation comparison of mathematical implementations for the dog-bone tension test. The $\sigma - \varepsilon$ curves agree well, while the $dt - t$ plot shows that the iterative numerical scheme is computationally demanding. It assures the computational compatibility of the proposed non-iterative scheme for speedier convergent results.

Please cite this article as:
V. Laheri, P. Hao, F.A. Gilabert.
"Efficient non-iterative modelling of pressure-dependent plasticity using paraboloidal yield criterion".
International Journal of Mechanical Sciences (2021), DOI: https://doi.org/10.1016/j.ijmecsci.2021.106988
Received: 18 Jul 2021, Revised: 25 Oct 2021, Accepted: 5 Dec 2021.

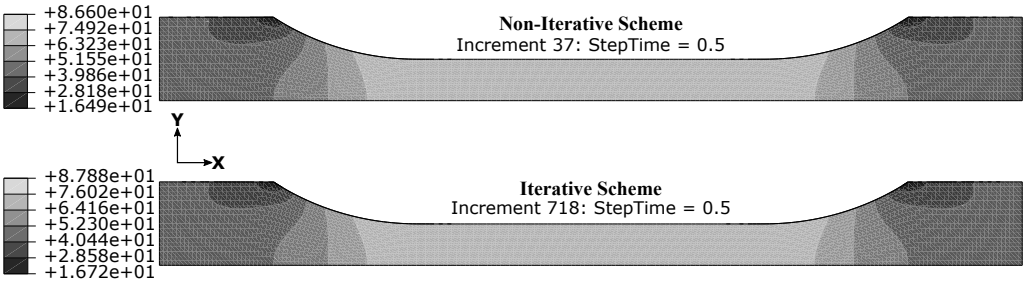

Figure 17: Max principal stress contour plot on the dog-bone specimen showing uniformly similar distribution of stress for classical iterative and proposed non-iterative numerical schemes.

Please cite this article as:
V. Laheri, P. Hao, F.A. Gilabert.
"Efficient non-iterative modelling of pressure-dependent plasticity using paraboloidal yield criterion".
International Journal of Mechanical Sciences (2021), DOI: https://doi.org/10.1016/j.ijmecsci.2021.106988
Received: 18 Jul 2021, Revised: 25 Oct 2021, Accepted: 5 Dec 2021.

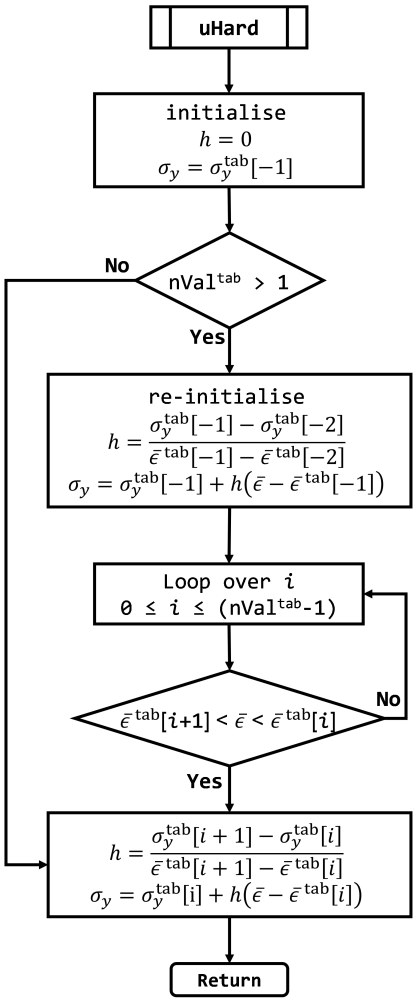

Figure 18: Piecewise linear hardening modulus computation algorithm.